International Journal of Greenhouse Gas Control 151 (2026) 104612

Contents lists available at ScienceDirect

International Journal of Greenhouse Gas Control

journal homepage: www.elsevier.com/locate/ijggc

Removal of CO from pre-combustion CO_2 rich streams using chemical looping technology

Dora-Andreea Chisăliță *, Gerard Douwe Elzinga, Jurriaan Boon

TNO Energy and Materials Transition, Sustainable Technologies for Industrial Processes, Westerduinweg 3, NL-1755LE Petten, the Netherlands

ARTICLE INFO

Keywords:
CO_2 purification
CO_2 quality
Impurities
Chemical looping
Energy recovery
Iron oxide

ABSTRACT

Complying with CO_2 purity specifications is unavoidable for any carbon capture technology due to technical, economic, and safety requirements for transportation, storage, and utilization. The tolerated impurity levels can be stringent, leading to a significant increase in capture costs. Depending on the applied technology and the flue gas source, different impurities are present. This study focuses on pre-combustion capture CO_2 purification, in particular removing CO using chemical looping technology. Compared to existing CO removal methods, chemical looping can remove CO with reduced energy penalty while at the same time improve the CO_2 recovery and remove other impurities like H_2 and CH_4 which might be present in pre-combustion CO_2 captured stream. The feasibility of applying chemical looping for deep CO removal (<100 ppm) was first evaluated thermodynamically, considering various oxygen carriers like Ni, Cu, Mn, and Fe. Promising redox couples identified include Cu_2O/Cu and Fe_2O_3/Fe_3O_4, while nickel and manganese based oxides showed less potential. Both reduction and regeneration are exothermic, offering opportunities for heat recovery. Iron-based oxygen carriers were further evaluated experimentally, showing excellent performance and stability over ~200 cycles at 400–550 °C for a 20wt%Fe_2O_3 impregnated on Al_2O_3 sample. Higher temperatures showed increased conversion up until 450 °C. Optimal operating temperatures should consider process design and economics, including heat integration options. CO_2 purification by chemical looping appears to be an attractive CO removal technology.

1. Introduction

Carbon Capture and Storage (CCS) is one of the key solutions acknowledged by the International Panel on Climate Change (IPCC) in tackling the climate crisis and contribute to achieve the Paris Agreement targets of limiting temperature increase to 1.5 °C (IPCC, 2023). It plays an important role in the clean energy transition by enabling emissions reduction from hard-to-abate sectors (e.g., steel, cement, chemicals) as well as facilitating cost-effective low-carbon hydrogen production (IEA, 2024). CCS involves the capture of CO_2, which can be accomplished by several technologies, the most investigated ones being pre-combustion, oxy-fuel combustion, post-combustion. Extensive descriptions of these technologies can be found in literature (Jansen et al., 2015; Monteiro et al., 2024; Zhao et al., 2023). The captured CO_2 if not used will be compressed and transported (by pipeline, ship, rail or truck) to be stored in various geological formations (such as depleted oil and gas reservoirs, saline aquifers, mineralization) (IEA, 2024; Zhao et al., 2023). Alternatively, the captured CO_2 can be used for the production of chemicals and fuels, also known as Carbon Capture Utilization (CCU). The purity of the captured CO_2 is an important criteria for any carbon capture technology due to technical, economic and safety requirements for transportation, storage, and utilization. The influence of the main impurities on the different sections the CCS/CCU chain are reviewed by (Wang et al., 2020) and reproduced in Table 1. The type of impurities greatly depends on the source of the CO_2 stream as well as on the capture technology employed. A comprehensive review of the impurities observed downstream of the main CO_2 capture technologies can be found in (Porter et al., 2015) and (Vitali et al., 2022). Additionally, depending on transportation mode and the destination of the CO_2 stream (e.g. storage, utilization), different purity requirements apply as

Abbreviations: CCS, Carbon Capture and Storage; CCU, Carbon Capture Utilization; CLC, Chemical looping combustion; EOR, Enhanced oil recovery; HSE, Health safety and environmental; IPCC, International panel on climate change; OC, Oxygen carrier; TGA, Thermogravimetric analysis; WGS, Water gas shift; CEM, Controlled evaporation mixer.

* Corresponding author.
E-mail address: dora.chisalita@tno.nl (D.-A. Chisăliță).

https://doi.org/10.1016/j.ijggc.2026.104612
Received 22 January 2025; Received in revised form 21 January 2026; Accepted 18 February 2026
Available online 27 February 2026

Table 1
Review of the influence of impurities on the different sections of the CCS/CCU chain by (Wang et al., 2020).

	High	Medium	Neutral
Compression	H_2	CH_4, N_2, CO, O_2, Ar	SO_2
Transportation	H_2O, SO_2, CO, NO_x, H_2S, O_2, H_2	N_2, Ar	CH_4
Storage	SO_2, CO, NO_x, H_2S, H_2O	N_2, Ar	CH_4
Utilization/ Conversion	SO_x, NO_x	-	-

Table 2
CO_2 specifications based on application.

	Unit	Transport (ship) & storage (Northern Lights, 2024)	Transport (pipeline) & storage - NETL (Shirley and Myles, 2019)	Pipeline transport for EOR - NETL (Shirley and Myles, 2019)	Pipeline transport for EOR - Weyburn (Brownsort, 2019)
H_2O	ppm	30	500	500	20
O_2	ppm	10	10	10	50
SOx	ppm	10	100	100	N/A
NOx	ppm	1.5	100	100	N/A
H_2S	ppm	9	100	100	9000
CO	ppm	100	35	35	1000
H_2	ppm	50	40,000	10,000	N/A
CH_4	ppm	100	40,000	10,000	7000
N_2	ppm	50	40,000	10,000	300
Amine	ppm	10	N/A	N/A	N/A
NH_3	ppm	10	50	50	N/A

exemplified in Table 2. As a result, additional purification steps are generally rEq.uired to meet these specifications, leading to supplementary cost. A solution would be to carefully match the type of CO_2 capture technology with the desired application, as the type and level of impurities are related to the CO_2 capture option (Wang et al., 2020). However, this is not always feasible since flue gases can significantly vary as a function of input raw material. Another consideration is the residual energy content of some of the impurities such as CO, H_2 or CH_4. While this may be recovered, this is scarcely taken into account when purification options are considered.

In the present study the focus is on the removal of CO from CO_2 rich streams. Different options are proposed in literature for removing CO depending on the initial concentration and the targeted destination of the CO_2 stream. For streams with CO_2 purity >80mol %, cryogenic separation can be employed to separate CO together with other non-condensable species. The downside is the large energy consumption due to the reduced temperatures rEq.uired (i.e., −10 to −60 °C) (Porter et al., 2021). Catalytic oxidation is another option, but accurate control of the oxygen feed is essential for not introducing new impurities, such as oxygen, and nitrogen in the case air is used instead of pure oxygen (Bilsbak, 2009). Another option is the conversion of CO to other products that can be more easily separated (Porter et al., 2021). One option is to convert CO to CO_2 through the water-gas-shift (WGS) reaction. This option would increase the CO_2 recovery but would rEq.uire both high and low temperature conversion units for deep CO removal as well as subsEq.uent H_2 removal. Methanation can be another alternative, converting CO to CH_4 which, similar to the WGS reaction, rEq.uires subsEq.uent separation of CH_4. To the best of our knowledge no purification option is available for efficient and effective removal of CO from CO_2 rich streams while at the same time not introducing new impurities in the process. Therefore, alternate solutions are rEq.uired. In the present study, chemical looping is proposed as a CO_2 purification technology for CO removal, increasing the CO_2 recovery as well as having the potential to remove other impurities such as H_2 and CH_4 in the same step. Chemical looping technologies have been mostly studied for fossil fuel conversion with CO_2 capture through chemical looping combustion (CLC) (Abuelgasim et al., 2021; Czakiert et al., 2022), but also other applications have shown great potential such as air separation (Cai et al., 2024; Krzystowczyk et al., 2021), hot liquid utility generation (Faizal and Deshpande, 2025), blue hydrogen production (Chisalita and Cormos, 2019; Ramezani et al., 2023) and chemicals production (Najera et al., 2011; Zhu et al., 2020). None of the evaluated applications for chemical looping look into the potential application for CO_2 purification. Furthermore, chemical looping studies reported in literature generally focus on high temperature operation of the process ($T > 800$ °C) and higher gas concentrations (e.g., 15–30 %) (Abad et al., 2007; Gallucci et al., 2015; Liu et al., 2014; Mattisson et al., 2007). In contrast, the proposed process would operate in a lower temperature regime (i.e., <700 °C) as well as with significantly lower reducing gas concentrations (i.e., <5 %). The goal of this study is to evaluate thermodynamically and experimentally the feasibility of applying chemical looping for CO removal from a CO_2 rich stream.

Table 3
General reactions taking place in the chemical looping process.

Conversion	Regeneration
$\mathbf{Me_XO_Y + CO \rightarrow Me_XO_{Y-\delta} + CO_2}$	$2Me_XO_{Y-\delta} + O_2 \rightarrow 2Me_XO_Y$
$\mathbf{Me_XO_Y + H_2 \rightarrow Me_XO_{Y-\delta} + H_2O}$	$Me_XO_{Y-\delta} + H_2O \rightarrow Me_XO_Y + H_2$
$\mathbf{4Me_XO_Y + CH_4 \rightarrow 4Me_XO_{Y-\delta} + CO_2 + 2H_2O}$	$Me_XO_{Y-\delta} + CO_2 \rightarrow Me_XO_Y + CO$

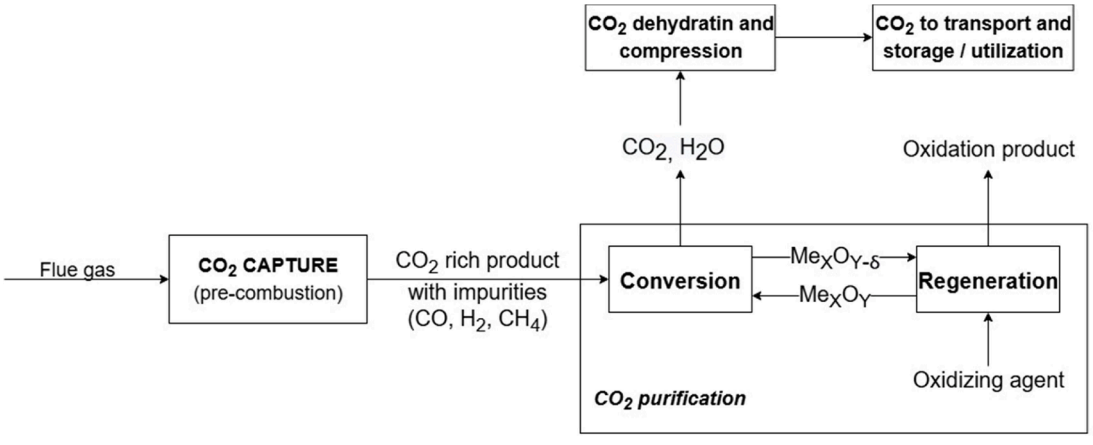

Fig. 1. Schematic representation of chemical looping purification technology in the CO2 capture system.

1.1. Process description

The proposed system is envisioned to be placed downstream the CO_2 capture with the aim of reaching CO_2 purity specifications for CO_2 transport and storage/utilization as shown schematically in Fig. 1. The chemical looping process takes place in two separate steps, conversion and regeneration, between which an O_2 transfer is performed via a metal oxide commonly known as oxygen carrier (OC). The general reactions that can take pace in each of the two steps is reported in Table 3. In the conversion step the OC is reduced by the incoming impurities which in turn are oxidized to CO_2 and water vapor, generally separated by condensation. In the second step, the reduced OC is regenerated by feeding a suitable oxidizing agent such as oxygen from air, steam, or CO_2. The outlet gas stream of the oxidation step contains mainly nitrogen and unreacted oxygen in the most typical case when air is used as oxidising agent. Heat and /or electricity can also be generated as a result of the exothermic nature of this step (Fan et al., 2015). When steam is used as an oxidation agent, pure hydrogen can be obtained as a by-product. Using CO_2 to regenerate the reduced oxygen carrier, the outlet will contain mainly CO. However, due to the weak oxidation capabilities of H_2O and CO_2, leading to slow and insufficient oxidation, an additional oxidation step with air is rEq.uired, which is generally the preferred oxidizing agent (Tang et al., 2015).

1.2. Oxygen carriers

Oxygen carriers are the most important aspect of any chemical looping process as their performance dictates the efficiency, costs and operating conditions of the process (Liu et al., 2022; Ramezani et al., 2023). Oxygen carriers are metal oxides capable of undergoing multiple reduction-oxidation cycles acting as reaction intermediates by providing the oxygen rEq.uired for conversion without introducing other impurities in the system. Ideal OC materials must have specific properties, such as high reactivity for both oxidation and reduction, low tendency to agglomeration, resistance to attrition and sintering in order to withstand multiple cycles, have a satisfactory oxygen transfer capacity, be non-toxic and environmentally benign and have a low cost (Fennell, 2015). In the last decades, various materials have been evaluated for their performance as OC, predominantly based on nickel (Ni), copper (Cu), manganese (Mn) and iron (Fe) oxides (Abuelgasim et al., 2021; Lyngfelt et al., 2019). Most of the early research concerning OC materials focused on NiO, mainly due to its high reactivity with methane. However, due to health, safety and environmental (HSE) risks associated with Ni-based materials as well as the high cost, the research shifted towards more environmentally friendly materials with lower cost (Mattisson et al., 2018). Copper-based materials are less costly and slightly less toxic than those based on Ni, but still more expensive than Mn and Fe-based materials, as copper ores have a low Cu percentage (Czakiert et al., 2022; Lyngfelt, 2015). Oxygen carriers based on CuO present high reactivity towards CH_4 and syngas, high oxygen transfer capacity as well as exothermic reduction reactions (Lyngfelt, 2015; Nandy et al., 2016). A main drawback is the low melting point of Cu (i.e. 1079 °C), which rEq.uires the process to be operated at lower temperatures (e.g. 800–850 °C) to avoid agglomeration of the OC particles (Lyngfelt, 2015). (Khan and Shamim, 2017) reported that sintering of materials due to temperature usually occurs at 70–80 % of their melting temperature, which means that sintering and agglomeration of Cu-based materials could be avoided in the proposed application. Mn-based OCs present high reactivity with syngas (CO, H_2), have a lower oxygen transport capacity than Ni and Cu but higher than Fe, are less likely to agglomerate, are non-toxic and significantly cheaper than Ni and Cu OCs (Czakiert et al., 2022; Lyngfelt, 2015; Nandy et al., 2016). Nonetheless, Mn-based OCs are the least studied materials (Abuelgasim et al., 2021). Iron-based OCs exhibit lower oxygen transfer capacity as well as lower reactivity towards gaseous fuels (CH_4 in particular); however, they present acceptable reactivity towards syngas, show low tendency to agglomeration and carbon formation, are the least expensive and do not present HSE risks (Nandy et al., 2016; Tang et al., 2015). Considering application in the steel sector, spent OC can be feed to the steelmaking process making it a circular material. Despite its lower reactivity, iron-based OCs have been extensively applied and studied in various chemical looping applications (Yu et al., 2019) and will be the focus of the present study as well.

In general, OCs are supported on an inert material for increased mechanical strength as well as for enhanced reactivity as pure metal oxides do not meet all the desired criteria for an efficient OC (Nandy et al., 2016). An extensive study was carried out by (Adánez et al., 2004), covering 240 samples of oxygen carriers prepared by mechanical mixing containing between 40 % and 80 % Cu, Fe, Mn or Ni oxides supported on various inert materials such as Al_2O_3, SiO_2, TiO_2, ZrO_2. Reactivity and mechanical strength was assessed in a TGA using methane (70 %CH_4 and 30 %H_2O) as fuel at 950 °C for all oxygen carriers except for those based on Cu which were carried out at 800 °C. Based on the results of the study, the authors recommend the use of SiO_2 or TiO_2 support for Cu-based oxygen carriers, Al_2O_3 or ZrO_2 for Fe-based oxygen carriers. ZrO_2 and TiO_2 lead to the best results for Mn and Ni-based materials respectively. In a follow-up study published by (Mattisson et al., 2007), the conversion of syngas to CO_2 and H_2O was also evaluated. Complete conversion of CO, H_2 and CH_4 were observed at 800 °C and 1000 °C for Fe, Cu and Mn-based oxygen carriers. However, not all redox couples based on Fe and Mn (i.e., $Fe_3O_4/Fe_{0.945}O$, MnO/Mn) showed complete conversion. Similarly, various metal oxides based on Ni, Cu, Fe, Mn, Co, W and sulphates of Ba and Sr were evaluated thermodynamically by (Jerndal et al., 2006) for their suitability as oxygen carriers for CLC using CH_4, CO and H_2 as fuel at temperatures of 800 °C and 1000 °C. Out of the evaluated oxygen carriers only metal oxides based on Cu, Fe and Mn showed complete conversion of the selected fuel**.** Oxygen carriers based on natural ores were also evaluated and are regarded as attractive options as a result of their abundance, lower environmental impact, and cost. A review was prepared by (Matzen et al., 2017) comparing the performance of various natural OC based on Fe, Mn, Cu and Ca ores against conventional synthetic OC. Iron ores, ilmenite in particular showed most promise due to its mechanical strength and stability. Mixed ores show also improved efficiencies. A sample containing 75 % ilmenite and 25 % Mn_2O_3 was evaluated by (Gallucci et al., 2015) in pressurized chemical looping combustion of syngas, showing good stability even at high active material content.

For the envisioned application it is essential that high selectivity, very close to unity is achieved, meaning high conversion of CO at lower temperatures than the conventional CLC process as most pre-combustion CO_2 capture technologies deliver the CO_2 rich stream at temperatures well below 700 °C (Theo et al., 2016).

2. Materials and methods

2.1. Thermodynamic evaluation

Thermodynamic evaluation of the proposed chemical looping purification process is an effective way to select suitable oxygen carriers that can completely convert CO under the relevant operating conditions as well as to assess heat integration possibilities. For a successful concept, both steps need to be thermodynamically feasible. Generally, studies covering thermodynamics of different OCs look only into high temperature operating window of 800 °C-1200 °C (Adanez et al., 2012; Jerndal et al., 2006), while in the intended application the focus will be on temperatures below 700 °C. Thus, the results of the thermodynamic evaluation will serve as a basis for selection of viable redox pairs under relevant conditions for the CO_2 purification process.

The thermodynamic evaluation was performed based on the second law of thermodynamics by analysing the change in Gibbs free energy (ΔG) alongside changes in enthalpy (ΔH) using HSC Chemistry v5.11 software (Outokumpu Research Oy, 2002). All solids were modelled as

Table 4
OC redox reactions with CO.

Redox pair	Reduction with CO	Oxidation with air
NiO/Ni	$NiO + CO = Ni + CO_2$	$2Ni + O_2 = 2NiO$
CuO/Cu$_2$O	$2CuO + CO = Cu_2O + CO_2$	$2Cu_2O + O_2 = 4CuO$
CuO/Cu	$CuO + CO = Cu + CO_2$	$2Cu + O_2 = 2CuO$
Cu$_2$O/Cu	$Cu_2O + CO = 2Cu + CO_2$	$4Cu + O_2 = 2Cu_2O$
MnO$_2$/Mn$_2$O$_3$	$2MnO_2 + CO = Mn_2O_3 + CO_2$	$2Mn_2O_3 + O_2 = 4MnO_2$
MnO$_2$/Mn$_3$O$_4$	$3MnO_2 + 2CO = Mn_3O_4 + 2CO_2$	$Mn_3O_4 + O_2 = 3MnO_2$
MnO$_2$/MnO	$MnO_2 + CO = MnO + CO_2$	$2MnO + O_2 = 2MnO_2$
MnO$_2$/Mn	$MnO_2 + 2CO = Mn + 2CO_2$	$Mn + O_2 = MnO_2$
Mn$_2$O$_3$/ Mn$_3$O$_4$	$3Mn_2O_3 + CO = 2Mn_3O_4 + CO_2$	$4Mn_3O_4 + O_2 = 6Mn_2O_3$
Mn$_2$O$_3$/ MnO	$Mn_2O_3 + CO = 2MnO + CO_2$	$4MnO + O_2 = 2Mn_2O_3$
Mn$_2$O$_3$/ Mn	$Mn_2O_3 + 3CO = 2Mn + 3CO_2$	$2Mn + 1.5O_2 = Mn_2O_3$
Mn$_3$O$_4$/MnO	$Mn_3O_4 + CO = 3MnO + CO_2$	$6MnO + O_2 = 2Mn_3O_4$
Mn$_3$O$_4$/Mn	$Mn_3O_4 + 4CO = 3Mn + 4CO_2$	$3Mn + 2O_2 = Mn_3O_4$
MnO/Mn	$MnO + CO = Mn + CO_2$	$2Mn + O_2 = 2MnO$
Fe$_2$O$_3$/Fe$_3$O$_4$	$3Fe_2O_3 + CO = 2Fe_3O_4 + CO_2$	$4Fe_3O_4 + O_2 = 6Fe_2O_3$
Fe$_2$O$_3$/FeO	$Fe_2O_3 + CO = 2FeO + CO_2$	$4FeO + O_2 = 2Fe_2O_3$
Fe$_2$O$_3$/Fe	$Fe_2O_3 + 3CO = 2Fe + 3CO_2$	$2Fe + O_2 = 1.5Fe_2O_3$
Fe$_3$O$_4$/FeO	$Fe_3O_4 + CO = 3FeO + CO_2$	$6FeO + O_2 = 2Fe_3O_4$
Fe$_3$O$_4$/Fe	$Fe_3O_4 + 4CO = 3Fe + 4CO_2$	$3Fe + 2O_2 = Fe_3O_4$
FeO/Fe	$FeO + CO = Fe + CO_2$	$2Fe + O_2 = 2FeO$

pure components.

Different redox pairs are possible for each of the most common metals oxides used in chemical looping. Table 4 summarizes the reduction reactions with CO of the various OC redox couples as well as the oxidation reactions with air. The thermodynamic favourability was evaluated for all possible redox couples, while the Eq.uilibrium composition at isothermal and isobaric (1 bara) conditions of the 1st chemical looping step was first evaluated starting from the most oxidized form of the oxygen carrier considering an input gas composition of 5mol % CO, 45mol % CO_2 and 50mol % H_2O. The assumed feed composition was chosen for easy analysis of the experimental results while in practice, CO concentration from pre-combustion CO_2 capture would be in the range of 300–4000 ppm. Based on the chemistry of the process the authors believe that 5 % is representative for the behaviour in the range of 300–4000 ppm. Nevertheless, the Eq.uilibrium composition starting from a feed with low CO content was also evaluated, specifically for a feed containing 500 ppm CO, 85mol % CO_2, and 14.95mol % H_2O. Sufficient moles of Me_XO_Y are present in the 1st step to allow 100 % oxidation of the CO present in the feed. The composition of the reduced oxygen carrier in step 2 depends on the outlet of step 1. Also, in the 2nd step sufficient moles of oxidizing agent (i.e., O_2) are present to allow 100 % oxidation of $Me_XO_{Y-\delta}$.

2.2. Experimental evaluation

2.2.1. Materials

Four different types of samples were prepared and tested:

Sample 4) **Pure Fe_2O_3**: pure Fe_2O_3 powder from Thermo Scientific (99.999 %, −100 mesh) is pelletized using a manual press, the obtained tablets are crushed in a mortar and then sieved to obtain a sieve fraction of 0.212–0.425 mm.

Sample 2) **Fe_2O_3 supported on Al_2O_3 – mixed sieve fractions**: sieve fraction of Fe_2O_3 and Al_2O_3 were prepared in the same way as described in *Sample 1* and mixed together before filling in the reactor. Iron oxide from Thermo Scientific (99.999 %, −100 mesh) and α-Al_2O_3 powder from Alfa Aesar (99.99 %) was used in the preparation.

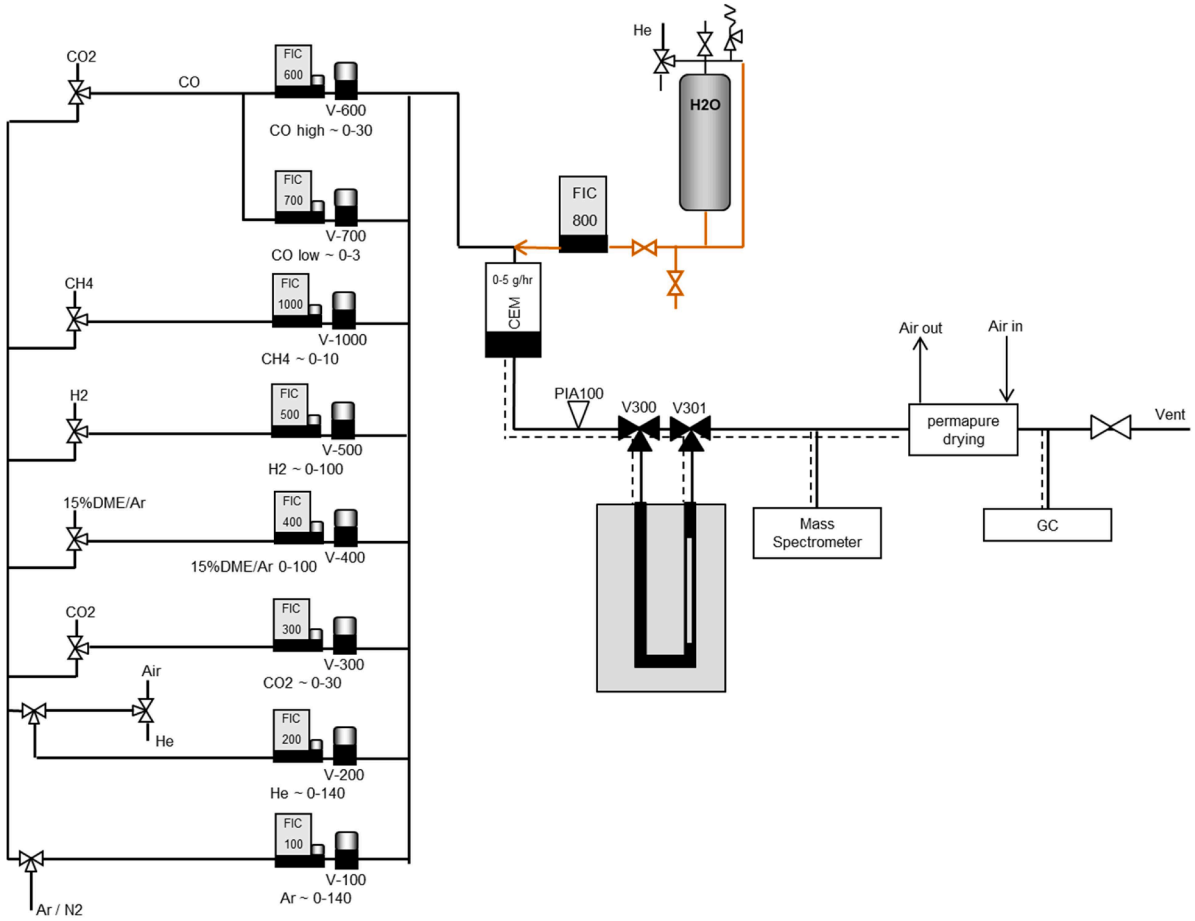

Fig. 2. Experimental setup.

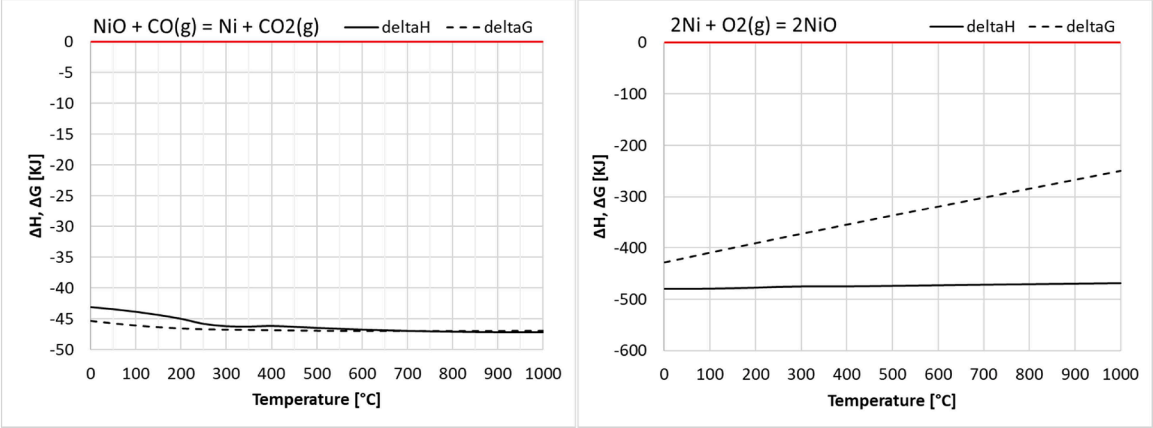

Fig. 3. Nickel oxide reduction with CO (left), Nickel oxidation with air (right).

Sample 3) **Fe_2O_3 supported on Al_2O_3 – mixed powders**: Fe_2O_3 powder from Thermo Scientific (99.999 %, −100 mesh) and α-Al_2O_3 powder from Alfa Aesar (99.99 %) were mixed thoroughly to an expected composition of 20wt % Fe_2O_3 on Al_2O_3 before pelletizing using a manual press; subsEq.uently the tablets were crushed and sieved to obtain the desired particle size of 0.212–0.425 mm.

Sample 4) **Fe_2O_3 supported on Al_2O_3 – impregnation**: 27.71 g Fe$(NO_3)_3 \cdot 9H_2O$ from Supelco (for analysis, Emsure ACS) is dissolved in demi water until a total volume of ~30 ml. The obtained solution is added bit by bit to 15.07 g γ-Al_2O_3 (Engelhard Al4170-p) in a mortar. In between the addition the mixture is mixed thoroughly. The final paste-like material is dried overnight at 120 °C and crushed until a fine powder was obtained. The powder was then calcined in air for 4 h at 700 °C which resulted in a yield of 15.66 g material with an expected composition of 20 %wt Fe_2O_3 on Al_2O_3. A sieve fraction was then made according to the previous mentioned procedure.

2.2.2. Experimental setup

Conversion-regeneration cycles were carried out in a lab-scale fixed bed unit illustrated in Fig. 2. The setup is Eq.uiped with a quartz reactor having an internal diameter of 10 mm for the pure Fe_2O_3 samples and 18 mm for the Fe_2O_3/Al_2O_3 materials. In case of pure Fe_2O_3 the sample mass of ~3.85 g results in a bed height of approximately 39 mm. For the Fe_2O_3/Al_2O_3 materials a total mass of 9 g (1.8 g Fe_2O_3) resulted in a bed height of 38–46 mm depending on the sample density. For lower CO concentration (i.e., 2000–4000 ppm) mesurements the mass of material was reduced to 3.026 g of material in order to keep the measurement times limited; a quarz reactor with internal diameter of 10 mm was used resulting in a bed heigth of 47 mm.

A series of Bronkhorst mass flow controllers is used to set the flow rates of the specific gases to get the final desired gas composition, and a Bronkorst liquiflow controller connected to a Controlled Evaporation Mixer (CEM) unit is used to subsEq.uently humidify the gas stream. Downstream the reactor a Pfeiffer MS is continuously measuring the outlet gas composition. For a more precise quantification a Varian CP-4900 micro GC is connected downstream the permapure gas dryer for one experimental run. All temperatures and flows are controlled and monitored by Control Maestro software.

The outlet gas composition was mainly measured using a MS which provides information about the molecules present in the stream based on their mass fragments. Information about the mass spectra for the molecules involved (i.e., CO, CO_2, H_2, H_2O) were taken from NIST Chemical database (US Department of Commerce, n.d.). Since the same mass can be observed in the spectra of more than one component, as is the case of mass 28 for CO and CO_2, an additional correction step is necessary. To evaluate the contribution of mass 28 to CO_2 an initial measurement with no CO in the feed was done at the beginning of each experiment. For quantification of the converted CO, the share of mass 28 in CO_2 was subtracted from the measured 28 mass signal.

To convert MS signals to flow and concentration additional calculations were necessary. Feed flows with three varying CO and CO_2 concentrations were measured at the beginning of each experiment keeping the total flowrate constant. Next, considering a linear dependence between input concentration and signal, the obtained corelation was used to evaluate the concentration for different signals. Finally, normalization with respect to Ar was applied. This was necessary to account for any drift that may happen in the MS signals in time (e.g., change in ambient pressure).

3. Results and discussion

3.1. Thermodynamic study results

3.1.1. Nickel oxide

For nickel oxide there is only one possible redox pair, NiO/Ni. Fig. 3 shows the change in Gibbs free energy and the change in enthalpy for the reduction of NiO with CO and the oxidation of Ni with air. Both steps are thermodynamically favourable and exothermic.

The Eq.uilibrium composition of the 1st chemical looping step is illustrated in Figure S1 (in Supplementary information) for the solid and gaseous phase. The solid phase composition at the end of the reduction step consists of Ni and unconverted NiO depending on the operating temperature. For the gaseous phase, by considering a molar ratio of NiO/CO=1, full oxidation of CO to CO_2 is thermodynamically achievable only at temperatures below 250 °C as also indicated by the incomplete NiO conversion above this temperature. The possibility of increasing the CO conversion by adding excess NiO in the 1st step was also evaluated. Two different NiO/CO molar ratios of 2 and 3 were assessed but without seeing any difference as it can be seen by the overlapping curves in Figure S2. The conversion of CO decreases with temperature from 100 % at $T < 250$ °C to 97 % at 700 °C and further to 88 % at 1000 °C. Looking at the outlet gas phase composition illustrated in Figure S1 it can be noted that CO_2 and H_2O are slightly decreasing with temperature while H_2 and CO are slightly increasing. This indicates that some side reaction/s may take place in the evaluated temperature range. If we consider a dry feed (5mol %CO, 95mol %CO_2) thus only take into account the species participating in the reaction: NiO + CO(g) = Ni + CO_2(g), the observed CO conversion is the same regardless of the NiO/CO ratio. Going from a wet feed to a dry feed seems to reduce the conversion as observed in Figure S2. If we look at a case where the inlet composition stays the same but H_2O is replace by an innert material resulting in a inlet feed composition of 5mol %CO, 45mol %CO_2 and 50mol %N_2 (noted dry* in Figure S2), we see that the CO conversion overlays with that observed in case of wet feed; having a higher CO_2

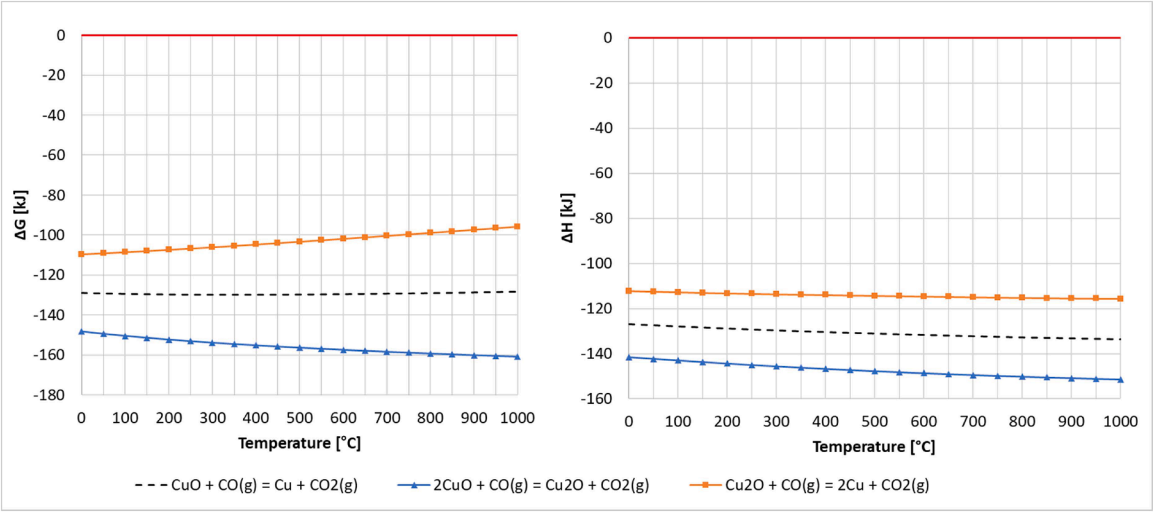

Fig. 4. Copper oxide reduction with CO.

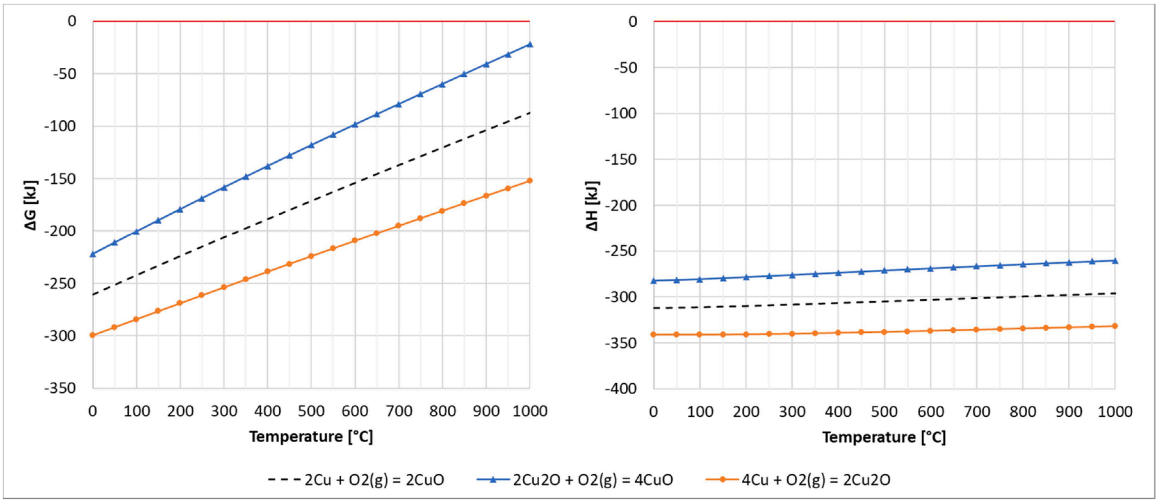

Fig. 5. Copper oxide oxidation with air.

concentration in the feed reduces the conversion of CO at higher temperature indicating that the reduction of NiO with CO may be Eq. uilibrium-limited. Since conversion of CO to the imposed specification limits cannot be achieved in the entire temperature range of interest (<700 °C) and for high CO_2 concentrations, the use of NiO for CO separation from a concentrated CO_2 stream will not be considered further.

3.1.2. *Copper oxide*

The evaluation of the possible reactions occurring in the reduction step of the Cu-based chemical looping with CO is illustrated in Fig. 4. All redox pairs are thermodynamically favoured and exothermic in the evaluated temperature interval, with CuO/Cu_2O being the most favourable. Similarly, the oxidation step with air is thermodynamically favourable for all redox pair (Fig. 5). Both the reduction and the oxidation step are exothermic so no additional energy input would be rEq.uired and there is energy recovery potential.

The Eq.uilibrium composition of the 1st chemical looping step was found to be dependent on the CuO/CO molar ratio. For CuO/CO=1 the gas and solid phase will consist of 100mol % Cu. If CuO/CO=2, the solid phase composition changes and it will be composed of 100mol % Cu_2O. In the case of CuO/CO=3 the solid phase composition will most likely be composed of 50mol % Cu_2O and the rest excess CuO. Reduction of CO concentration bellow the imposed specification of 100 ppm (i.e., Northern Lights) can be achieved for all redox couples in evaluated temperature range, especially for CuO/Cu_2O redox pair. Gas and solid phase compositions for the evaluated molar ratios are illustrated in Figure S3 to Figure S5. The influence of the CO_2 concentration was evaluated considering a case with a higher CO_2 concentration, using a feed composition of 85mol %CO_2, 5mol %CO, 10mol %H_2O, shown in Figure S6 for the CuO/Cu redox pair. With increasing CO_2 concentration, the conversion of CO at higher temperatures (>650 °C) starts to decrease but it is still sufficient to reach the 100 ppm specification. For CuO/Cu_2O redox couple complete conversion of CO to CO_2 at high CO_2 concentration in the feed can be achieved at all evaluated temperatures as seen from Figure S7.

3.1.3. *Manganese oxide*

The variation of the Gibbs free energy and enthalpy of manganese oxide reduction with CO is illustrated in Fig. 6. The most thermodynamically feasible redox pair was found to be MnO_2/Mn_3O_4; Out of the ten evaluated redox pairs, three do not show thermodynamic feasibility in the forward direction ($\Delta G>0$), these are Mn_3O_4/Mn, Mn_2O_3/Mn, MnO/Mn. All the other redox pair show good promise in oxidizing CO to CO_2 from a thermodynamic point of view, in the following order $MnO_2/Mn_3O_4 > MnO_2/Mn_2O_3 > Mn_2O_3/Mn_3O_4 > MnO_2$/MnO > Mn_2O_3/MnO > Mn_3O_4/MnO > MnO_2/Mn. On the other hand, the oxidation of

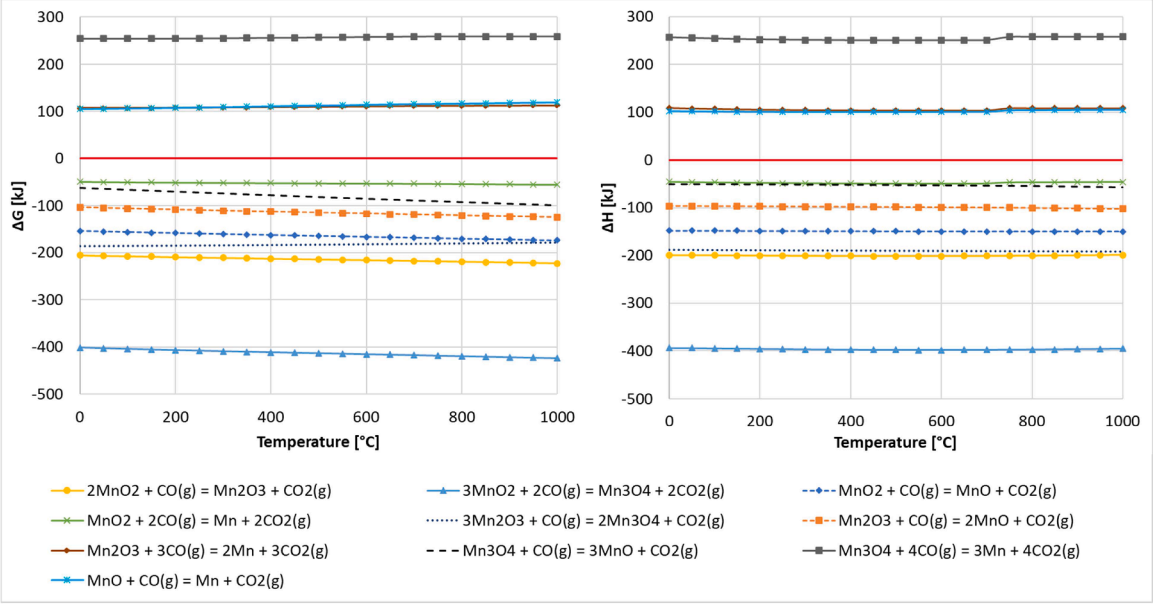

Fig. 6. Manganese oxide reduction with CO.

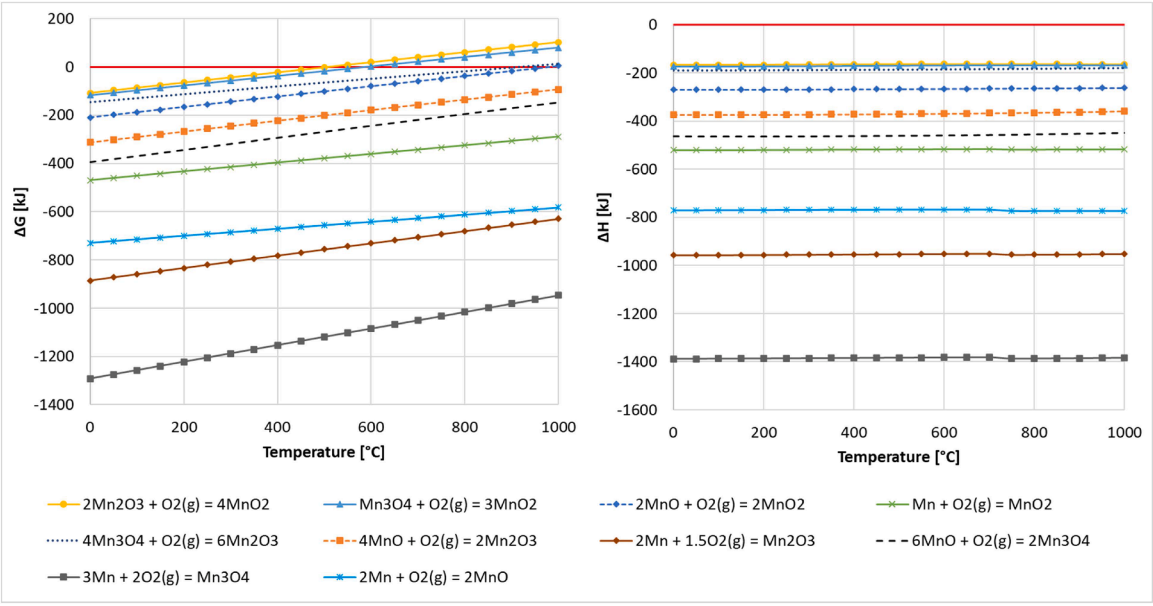

Fig. 7. Manganese oxide oxidation with air.

manganese oxides with air shows the opposite order as seen in Fig. 7. The redox pairs identified as being thermodynamically favoured for the oxidation of CO to CO_2 are not all thermodynamically favourable in the evaluated temperature range for oxidation with air. The preferred redox couple for reduction with CO, MnO_2/Mn_3O_4, is thermodynamically favoured for oxidation with air only at $T \leq 550$ °C which might be challenging to achieve since both steps are exothermic. Similarly, the next pair, MnO_2/Mn_2O_3 is thermodynamically favoured for oxidation with air only at $T \leq 500$ °C. The next two pairs Mn_2O_3/Mn_3O_4 and MnO_2/MnO are thermodynamically favoured for oxidation with air at $T \leq 900$ °C and $T \leq 950$ °C, respectively. The Eq.uilibrium composition starting from MnO_2 and Mn_2O_3 will be evaluated next.

Starting from MnO_2, the Eq.uilibrium composition during reduction with CO was evaluated at different MnO_2/CO ratios between 1 and 3. Figure S8 to Figure S11 show the Eq.uilibrium composition of the solid and gaseous phase. At MnO_2/CO=1 (i.e., MnO_2/MnO) the reduced phase will be MnO and conversion of CO to meet the imposed specification can be achieved in the entire temperature range evaluated. Small amounts of H_2 are observed together with Mn_3O_4 formation, indicating also the transition to a new solid phase at MnO_2/CO=1.5 (i.e. MnO_2/Mn_3O_4). Complete conversion of CO to CO_2 can be achieved in the entire temperature range and no H_2 formation is observed. At MnO_2/CO=2 and 3, the reduced solid phase will consist of Mn_2O_3 and excess MnO_2. Reduction of CO concentration to comply with specification can be achieved in the entire temperature range. Since in practice excess MnO_2 will most probably be used to ensure complete conversion of CO, in assessing the Eq.uilibrium composition during the regeneration step, the reduced form is considered to be 100 % Mn_2O_3. As seen in Figure S12 using excess O_2, complete oxidation of Mn_2O_3 to MnO_2 is only achieved at $T < 500$ °C as already indicated by the ΔG-T plot (see Fig. 7) thus

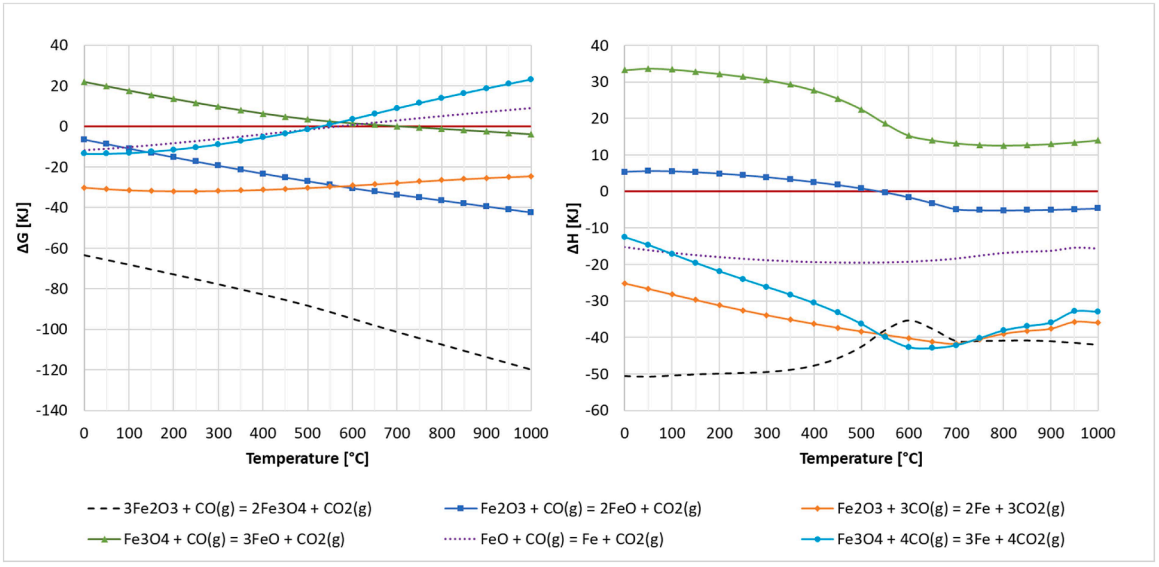

Fig. 8. Iron oxide reduction with CO.

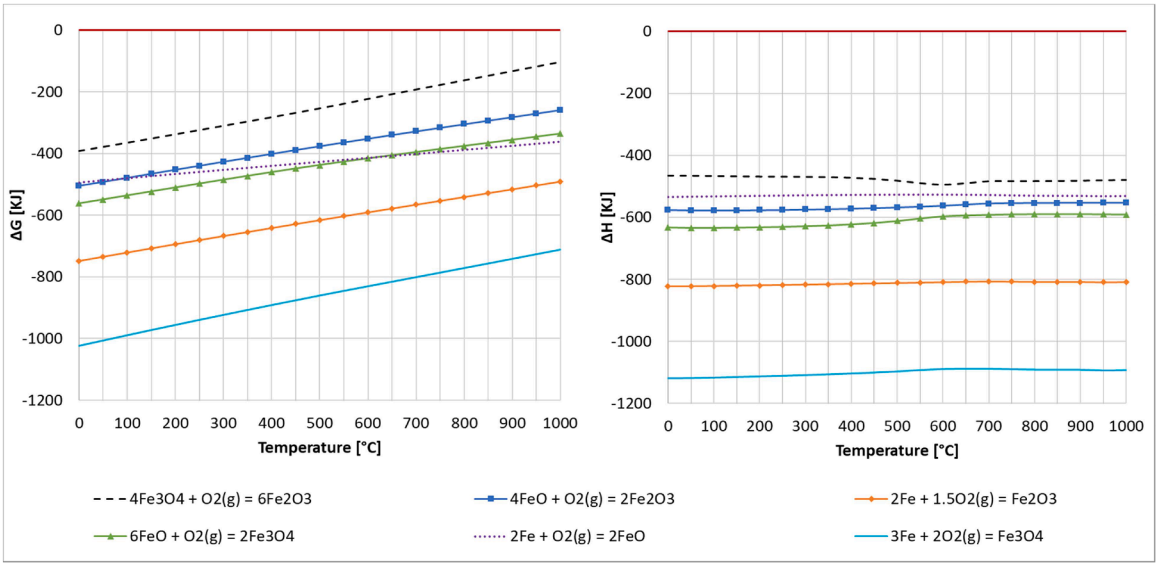

Fig. 9. Iron oxide oxidation with air.

making it not an ideal OC for the proposed application.

Starting from Mn_2O_3 the Eq.uilibrium composition at Mn_2O_3/CO=3 is represented in Figure S13. Complete conversion of CO is achieved in the evaluated temperature range. The reduced manganese oxide consists

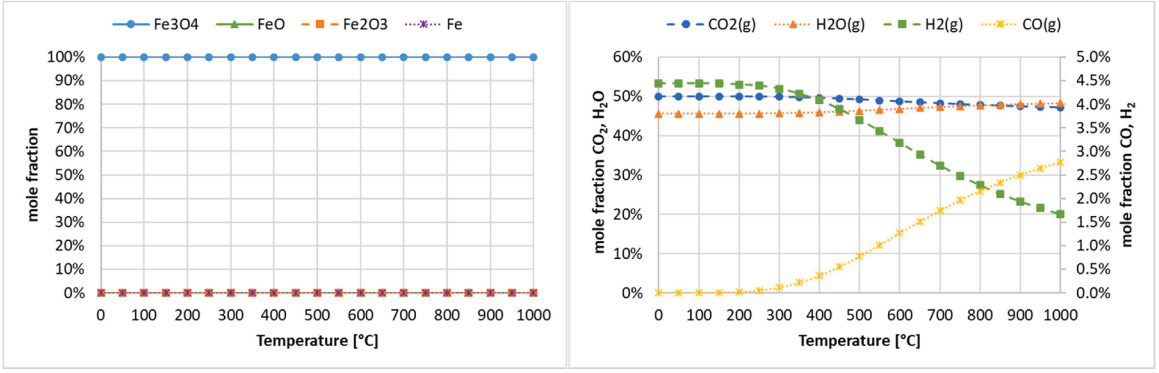

Fig. 10. Eq.uilibrium composition at Fe_2O_3/CO=1/3 at feed composition 5mol %CO, 45mol %CO_2, 50mol %H_2O.

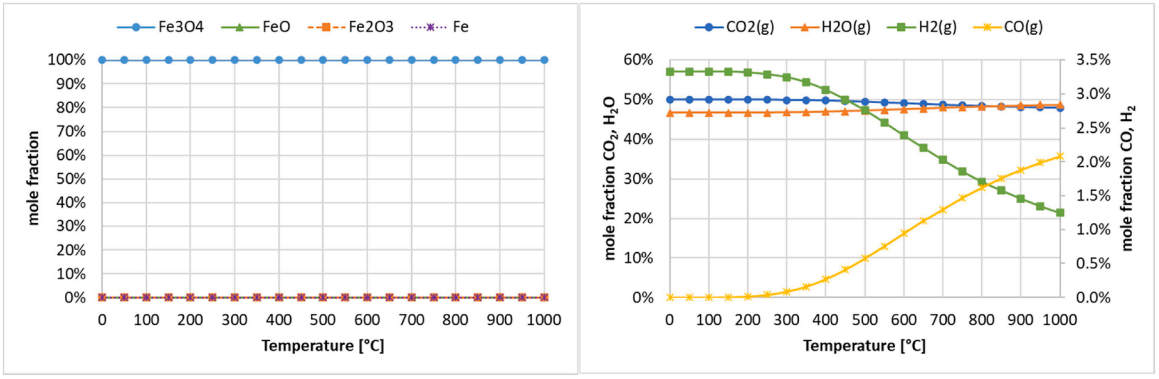

Fig. 11. Eq.uilibrium composition at Fe_2O_3/CO=1 at feed composition 5mol %CO, 45mol %CO_2, 50mol %H_2O.

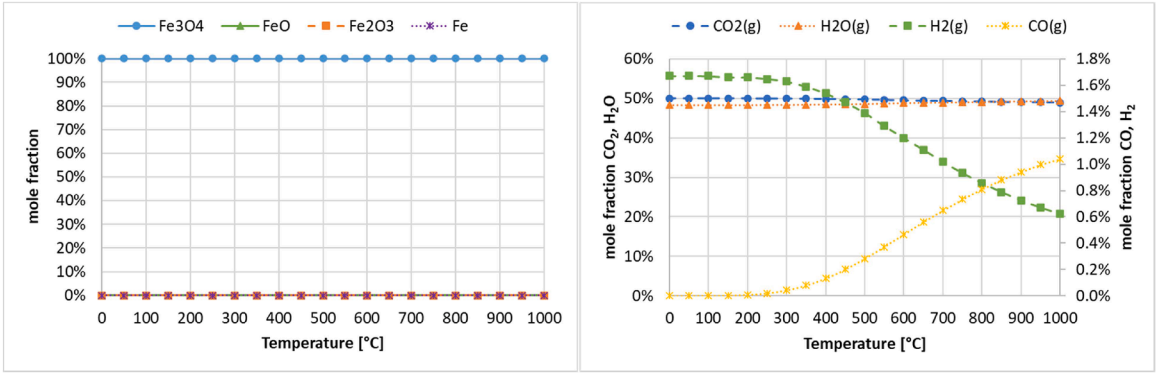

Fig. 12. Eq.uilibrium composition at Fe_2O_3/CO=2 at feed composition 5mol %CO, 45mol %CO_2, 50mol %H_2O.

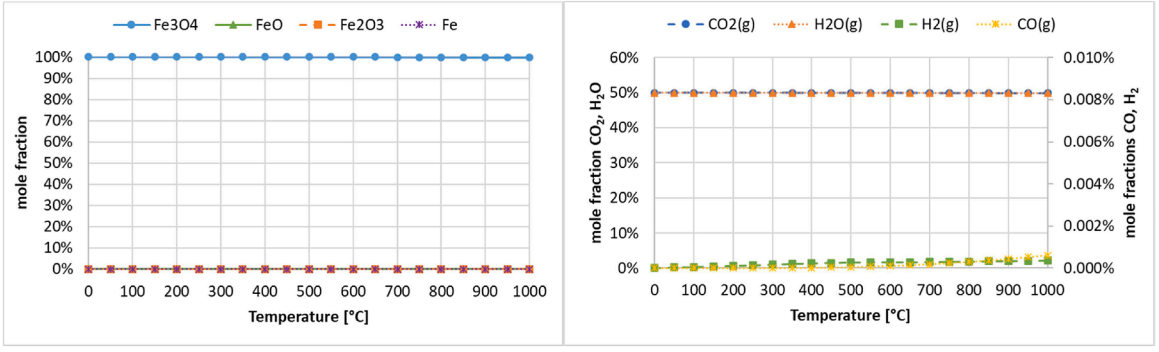

Fig. 13. Eq.uilibrium composition at Fe_2O_3/CO=3 at feed composition 5mol %CO, 45mol %CO_2, 50mol %H_2O.

of 100 % Mn_3O_4, which as seen from Fig. 7 is thermodynamically favoured for oxidation with air at temperatures up to 900 °C which would make for a feasible operation of the process.

3.1.4. Iron oxide

Fig. 8 shows the variation of the Gibbs free energy and enthalpy as a function of temperature for the reduction of iron redox with CO. The Fe_2O_3/Fe_3O_4 pair is thermodynamically favourable at all temperatures; Fe_2O_3/Fe, Fe_3O_4/Fe and FeO/Fe pairs are favourable at low temperatures, while Fe_2O_3/FeO is favourable at high temperatures. Both Fe_3O_4/Fe and FeO/Fe couples are spontaneous in the forward direction only at temperatures lower than 500 °C and 550 °C respectively, while Fe_3O_4/FeO is favourable in the forward direction only at temperatures higher than 750 °C, which is out of scope for the current application. Oxidation with air is thermodynamically favourable in the entire evaluated temperature range for all redox pairs as observed in Fig. 9.

Starting from the most oxidized form of Fe-based oxygen carrier (i.e., Fe_2O_3), the Eq.uilibrium composition of the 1st chemical looping step was evaluated at different Fe_2O_3/CO molar ratios from 1/3 to 4. It was found that irrespective of the Fe_2O_3/CO ratio, the reduced iron oxide will be Fe_3O_4. At Fe_2O_3/CO<3, hydrogen starts to form as well, lowering the conversion of CO as it can be seen from Figs. 10-14. Since iron oxide is also used as a catalyst for high temperature water-gas-shift (HT-WGS) at temperatures around 400 °C, the WGS reaction (Eq. (1)) may also occur in the reduction step as it can be noted in Figure S14, being a possible origin for the observed H_2 formation. Since in practice excess iron oxide will be used to guarantee high CO conversions, H_2 formation can be avoided and CO removal to comply with imposed specification can be achieved for the Fe_2O_3/Fe_3O_4 redox pair at all evaluated temperatures. The influence of CO_2 concentration was likewise evaluated considering the same feed composition as in the previous cases 5mol % CO, 85mol % CO_2 and 10mol % H_2O. The Eq.uilibrium composition of

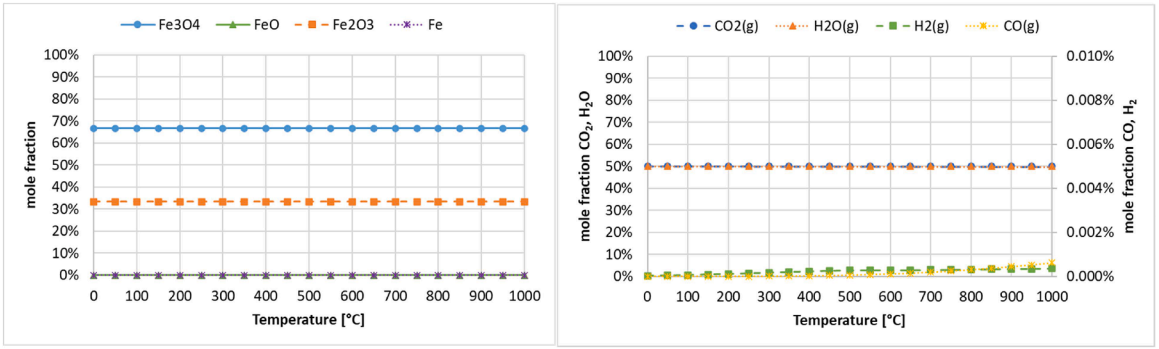

Fig. 14. Eq.uilibrium composition at Fe_2O_3/CO=4 at feed composition 5mol %CO, 45mol %CO_2, 50mol %H_2O.

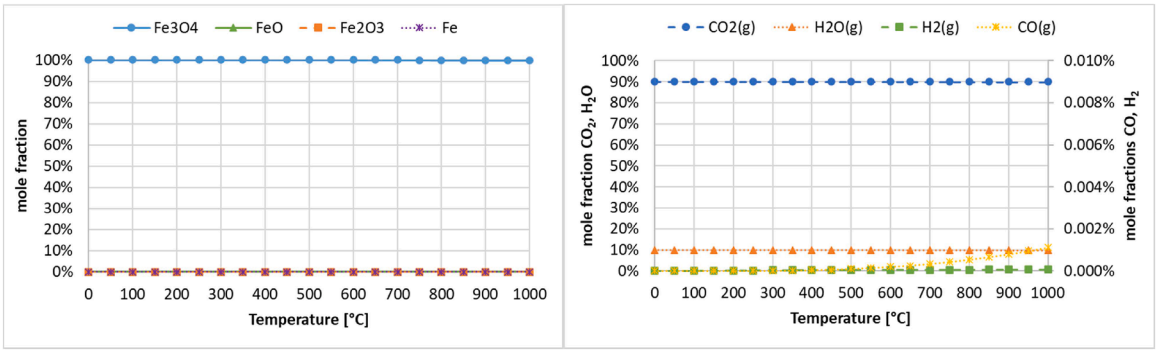

Fig. 15. Eq.uilibrium composition at Fe_2O_3/CO=3 at feed composition 5mol %CO, 85mol %CO_2, 10mol %H_2O.

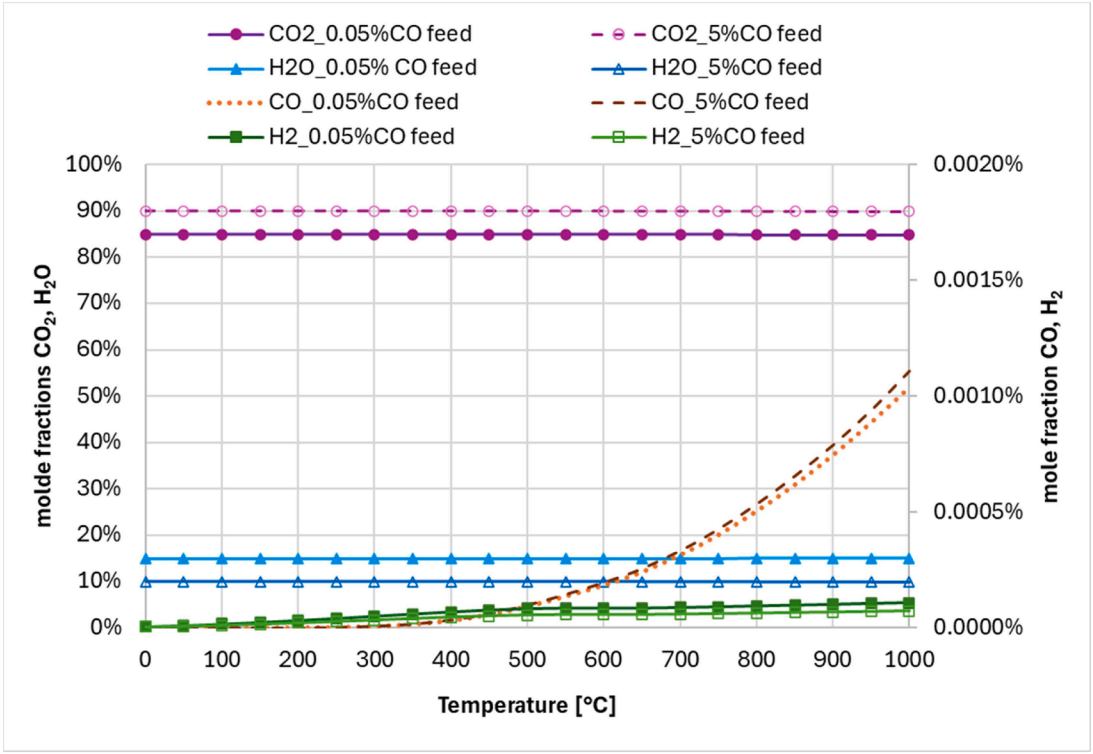

Fig. 16. Eq.uilibrium composition at Fe_2O_3/CO=3 at feed composition 500ppmCO, 85mol %CO_2, 14.5mol %H_2O and 5mol %CO, 85mol %CO_2, 10mol %H_2O.

the solid and gas phase is represented in Fig. 15 for Fe_2O_3/CO=3. CO removal from a concentrated CO_2 stream can be achieved using iron-based oxygen carrier meeting the specifications imposed on CO_2 purity. Additionally, the Eq.uilibrium composition of a feed containing lower CO content was evaluated for a feed containing 500 ppm CO, 85mol %CO_2 and 14.95mol % H_2O. As seen in Fig. 16, there is negligible

Table 5
Comparative summary on evaluated OCs performance and feasibility window based on the thermodynamic assessment.

Redox pair	Reduction with CO	Oxidation with air
NiO/Ni	* thermodynamically favourable at all T * exothermic: $\Delta H^0 = -43$ kJ/mol * CO conversion dependent on CO_2 content in feed * COout < 100 ppm at $T \leq 350$ °C	* thermodynamically favourable at all T * exothermic: $\Delta H^0 = -479$ kJ/mol
CuO/Cu_2O	* thermodynamically favourable at all T * exothermic: $\Delta H^0 = -142$ kJ/mol * expected redox pair when starting from excess CuO * COout < 100 ppm at all T	* thermodynamically favourable at all T * exothermic: $\Delta H^0 = -282$ kJ/mol
CuO/Cu	* thermodynamically favourable at all T * exothermic: $\Delta H^0 = -127$ kJ/mol * COout < 100 ppm at all T	* thermodynamically favourable at all T * exothermic: $\Delta H^0 = -312$ kJ/mol
Cu_2O/Cu	* thermodynamically favourable at all T * exothermic: $\Delta H^0 = -112$ kJ/mol	* thermodynamically favourable at all T * exothermic: $\Delta H^0 = -341$ kJ/mol
MnO_2/ Mn_2O_3	* thermodynamically favourable at all T * exothermic: $\Delta H^0 = -200$ kJ/mol * expected redox pair when starting from excess MnO_2 * COout < 100 ppm at all T	* thermodynamically favourable at $T \leq 500$ °C * exothermic: $\Delta H^0 = -166$ kJ/mol
MnO_2/ Mn_3O_4	* thermodynamically favourable at all T * exothermic: $\Delta H^0 = -394$ kJ/mol * COout < 100 ppm at all T	* thermodynamically favourable at $T \leq 550$ °C * exothermic: $\Delta H^0 = -172$ kJ/mol
MnO_2/ MnO	* thermodynamically favourable at all T * exothermic: $\Delta H^0 = -148$ kJ/mol * COout < 100 ppm at all T	* thermodynamically favourable at $T \leq 950$ °C * exothermic: $\Delta H^0 = -269$ kJ/mol
MnO_2/Mn	* thermodynamically favourable at all T * exothermic: $\Delta H^0 = -46$ kJ/mol	* thermodynamically favourable at all T * exothermic: $\Delta H^0 = -520$ kJ/mol
Mn_2O_3/ Mn_3O_4	* thermodynamically favourable at all T * exothermic: $\Delta H^0 = -188$ kJ/mol * expected redox pair when starting from excess Mn_2O_3 * COout < 100 ppm at all T	* thermodynamically favourable at $T \leq 900$ °C * exothermic: $\Delta H^0 = -190$ kJ/mol
Mn_2O_3/ MnO	* thermodynamically favourable at all T * exothermic: $\Delta H^0 = -96$ kJ/mol	* thermodynamically favourable at all T * exothermic: $\Delta H^0 = -373$ kJ/mol
Mn_2O_3/ Mn	* thermodynamically NOT favourable * endothermic: $\Delta H^0 = 109$ kJ/mol	* thermodynamically favourable at all T * exothermic: $\Delta H^0 = -957$ kJ/mol
Mn_3O_4/ MnO	* thermodynamically favourable at all T * exothermic: $\Delta H^0 = -51$ kJ/mol	* thermodynamically favourable at all T * exothermic: $\Delta H^0 = -464$ kJ/mol
Mn_3O_4/Mn	* thermodynamically NOT favourable * endothermic: $\Delta H^0 = 257$ kJ/mol	* thermodynamically favourable at all T * exothermic: $\Delta H^0 = -1388$ kJ/mol
MnO/Mn	* thermodynamically NOT favourable * endothermic: $\Delta H^0 = 103$ kJ/mol	* thermodynamically favourable at all T * exothermic: $\Delta H^0 = -771$ kJ/mol
Fe_2O_3/ Fe_3O_4	* thermodynamically favourable at all T * exothermic: $\Delta H^0 = -51$ kJ/mol * expected redox pair when starting from excess Fe_2O_3 * COout < 100 ppm at all T	* thermodynamically favourable at all T * exothermic: $\Delta H^0 = -464$ kJ/mol
Fe_2O_3/FeO	* thermodynamically favourable at all T	* thermodynamically favourable at all T
	* endothermic: $\Delta H^0 = 5$ kJ/mol * slightly exothermic from $T \geq 550$ °C	* exothermic: $\Delta H^0 = -576$ kJ/mol
Fe_2O_3/Fe	* thermodynamically favourable at all T * exothermic: $\Delta H^0 = -25$ kJ/mol	* thermodynamically favourable at all T * exothermic: $\Delta H^0 = -823$ kJ/mol
Fe_3O_4/FeO	* thermodynamically favourable at $T \geq 750$ °C * endothermic: $\Delta H^0 = 33$ kJ/mol	* thermodynamically favourable at all T * exothermic: $\Delta H^0 = -632$ kJ/mol
Fe_3O_4/Fe	* thermodynamically favourable at $T \geq 550$ °C * exothermic: $\Delta H^0 = -12$ kJ/mol	* thermodynamically favourable at all T * exothermic: $\Delta H^0 = -1119$ kJ/mol
FeO/Fe	* thermodynamically favourable at $T \geq 600$ °C * exothermic: $\Delta H^0 = -15$ kJ/mol	* thermodynamically favourable at all T * exothermic: $\Delta H^0 = -535$ kJ/mol

different in the observed Eq.uilibrium composition between a feed containing 5mol %CO and 500 ppm CO, indicating that the process is not Eq.uilibrium limited.

$$CO + H_2O \rightleftarrows CO_2 + H_2 \quad (1)$$

3.1.5. Carbon formation

During OC reduction, carbon formation may happen under certain conditions leading to poor stability and material deactivation (Ramezani et al., 2023). Depending on the feed composition, carbon formation can occur either from the Boudouard reaction (Eq. (2)), either from methane decomposition (Eq. (3)). As seen from Figure S15, the Boudouard reaction is thermodynamically favoured at low temperatures while carbon decomposition (in case there is CH_4 present in the feed) is favoured at high temperatures. Studies on carbon formation on iron-based oxygen carriers in chemical looping combustion of syngas have been previously carried out by various groups (Gallucci et al., 2015; Jerndal et al., 2006). A general conclusion is that carbon deposition depends on the amount of oxygen available and can be mitigated by feeding wet feed gas.

$$2CO \rightarrow C + CO_2 \quad (2)$$

$$CH_4 \rightarrow C + 2H_2 \quad (3)$$

Summarizing the results of the thermodynamic study, the performance and operating window for all evaluated redox pairs can be found in Table 5. The most promising redox pairs for feasible operation of the proposed chemical looping purification technology were identified as CuO/Cu_2O, Fe_2O_3/Fe_3O_4, and Mn_2O_3/ Mn_3O_4.

3.2. Experimental results

The experiments were done at atmospheric pressure in a cyclic mode with regeneration performed by switching the gas flow to air with an intermediate nitrogen flush. The diferent settings tested are summarized in Table 6, with flows defined at 25 °C and 1 atm.

Sample 1, pure iron oxide, is not stable enough to carry out multiple cycles as seen in Fig. 17. Complete conversion of CO can be observed only in case dry feed is used but the conversion time decreases as more cycles are run, going from cycle 2 to 15 the time for complete conversion decreases by about half. The performance of the process decreases with the number of cycles indicating stability issues most probably due to sintering. If pure iron will be used, frEq.uent change of material will be rEq.uired, and water needs to be removed from the CO_2 stream prior to this purification step.

To improve the stability issues, iron oxide supported on alumina was

Table 6
Chemical looing purification experimental settings.

Settings		Sample	No. of cycles	T [°C]	Time [min]	Feed flowrate [Nml/min]	Feed composition [mol %]				
							CO	CO_2	H_2O	Ar	Air
1.1	Conversion	Sample 1	15	400	120	60	5	45	-	50	
	Regeneration			400	15	60					100
1.2	Conversion		15	400	120	60	5	45	15	35	
	Regeneration			400	15	60					100
2.1	Conversion	Sample 2	15	400	240	30	5	45	-	50	
	Regeneration			400	15	30					100
2.2	Conversion		15	400	240	30	5	45	15	35	
	Regeneration			400	15	30					100
3.1	Conversion	Sample 3	15	400	240	30	5	45	-	50	
	Regeneration			400	15	30					100
3.2	Conversion		15	400	240	30	5	45	15	35	
	Regeneration			400	15	30					100
4.1	Conversion	Sample 4	115	400	100	60	5	45	15	35	
	Regeneration			400	15	60					100
4.2	Conversion		5 / T	250–400 450–550	100 150	60	5	45	15	35	
	Regeneration			250–550	15	60					100
4.3	Conversion		4	400	700	60	0.4	45	15	39.8	
	Regeneration			400	15	60					100
4.4	Conversion		4	400	700	60	0.2	45	15	39.6	
	Regeneration			400	15	60					100

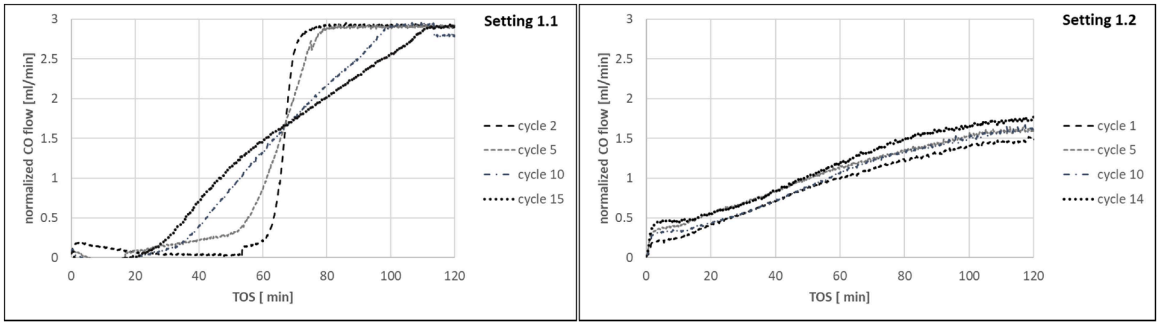

Fig. 17. Overlay of CO profile for 15 cycles of the first chemical looping step for Sample 1, for dry feed -Setting 1.1, and wet feed – setting 1.2.

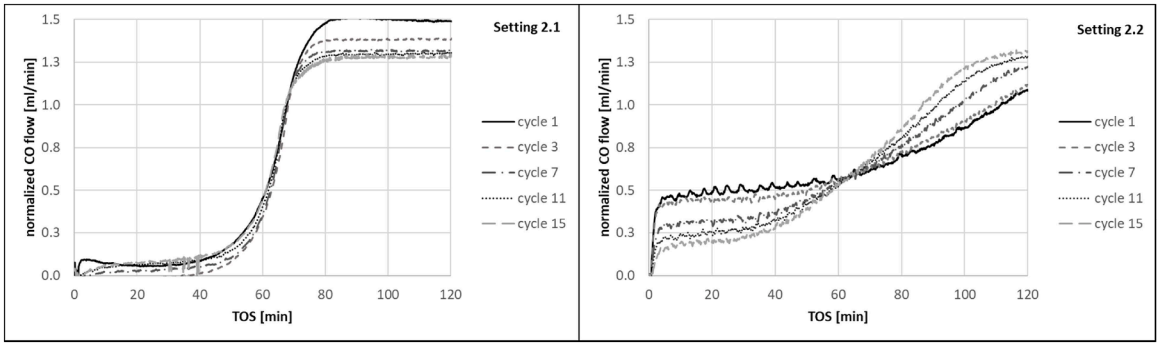

Fig. 18. Overlay of CO profile for 15 cycles of the first chemical looping step for Sample 2, for dry feed -Setting 2.1, and wet feed – setting 2.2.

evaluated next considering three different preparation methods, Sample 2, Sample 3 and Sample 4 as described in Section 2.2.1. The different samples exemplify different particle sizes for the iron oxide from larger to smaller. The results from the MS measurements during the first chemical looping step for the CO evolution for Sample 2 for wet and dry feed (Setting 2.1 and 2.2 in Table 5) is represented in Fig. 18. For a total of 15 cycles measured, good stability was observed for Sample 2 during dry feed as seen from the overlay of the CO profiles, while in case of wet feed this is not the case anymore. Complete conversion of CO to CO_2 can be achieved only for the dry feed for the first ~40 min after which the CO concentration starts to increase indicating a decrease in conversion. This is also an indication that the cycle time should be reduced when designing the process, stopping before CO concentration starts to increase. For the wet feed sufficient conversion levels are not reached. In case of Sample 3, a slightly improved stability is observed, for both dry and wet settings, and a longer conversion period for the wet feed as seen from Fig. 19. Similarly to Sample 2, in case of wet sample CO conversion is not enough to satisfy the imposed specification on CO allowed in the captured CO_2 stream, reaching only ~80 % in the first 40 min. Fig. 20 nicely shows the transient response during the fist 5 cycles and the carbon balance during CO oxidation to CO_2 – increase in CO_2 signal when CO conversion is high and a decrease in CO_2 signal when the CO

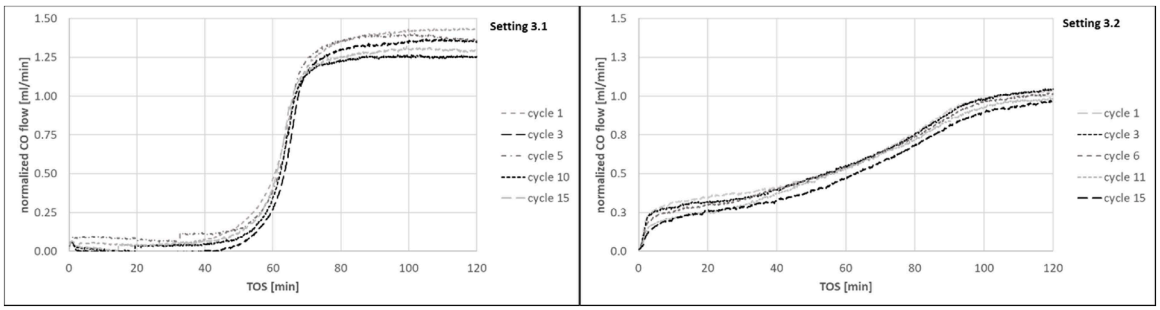

Fig. 19. Overlay of CO profile for 15 cycles of the first chemical looping step on Sample 3 for dry feed -Setting 3.1, and wet feed – setting 3.2.

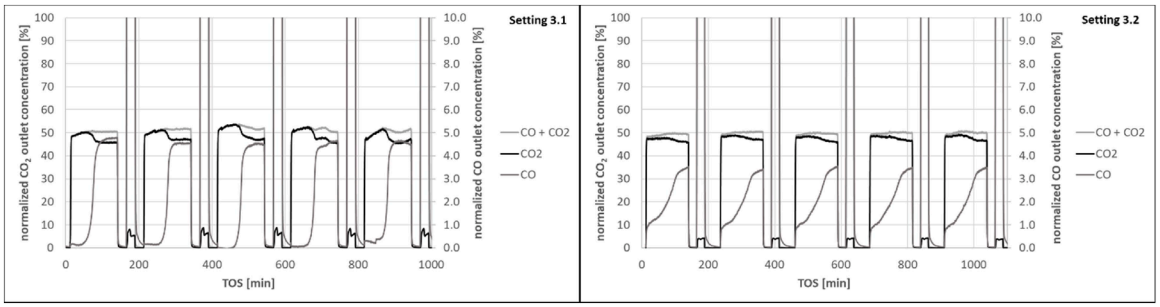

Fig. 20. Transient response of CO and CO_2 concentrations during the first chemical looping step on sample 3.

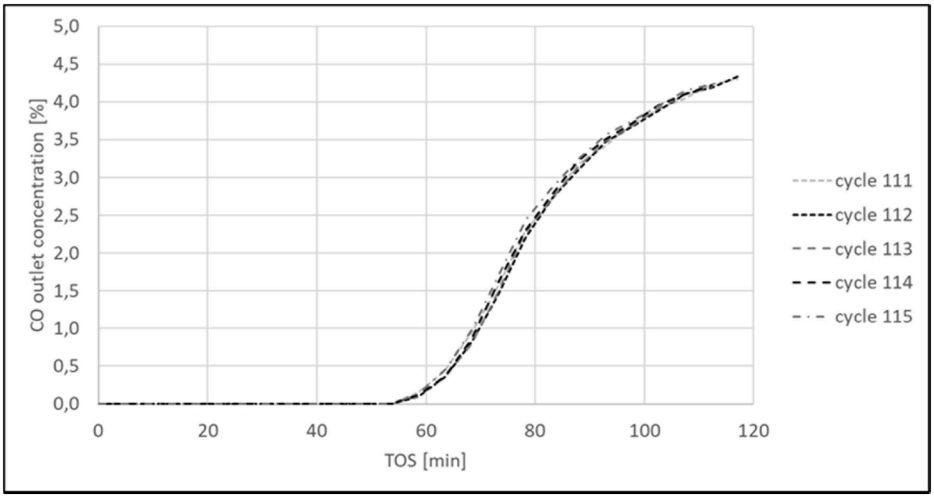

Fig. 21. Overlay of CO concentration for cycles 111 to 115 of the first chemical looping step measured with GC on Sample 4 – setting4.1.

conversion decreases.

For Sample 4, impregnated iron oxide on alumina, a total of 115 cycles were measured with wet feed for which the last 5 cycles were also measured with a GC to confirm the results from the MS measurements for complete conversion of CO. Fig. 21 and Fig. 22 show the results from the GC measurements during the first chemical looping step for the CO concentration evolution and the CO, CO_2 transient responses respectively. Complete conversion of CO to CO_2 is observed for the first ~50 min after which the CO concentration starts to increase, indicating the cycle time should be reduced in this case as well when designing the process. Excellent stability was observed for over 100 cycles as seen from the overlay of the CO profiles in Fig. 21 and consistent carbon balance. Fig. 22 shows the carbon balance during the CO oxidation to CO_2 for cycle 110–115.

The influence of a wet feed was evaluated from a thermodynamic perspective to identify possible reasons for the behaviour observed for samples 1 to 3. As reported in Figure S16 of the Supplementary information, the presence of H_2O in the feed does not impose any thermodynamic limitations. For Sample 4 water appears to have no negative effect on CO conversion, suggesting that the limitations are likely kinetic. A key difference among the prepared samples is the particle size of the iron oxide, which relates to the surface area and impacts reaction kinetics. The better results observed for Sample 4 could also be attributed to a more uniform iron oxide distribution as a results of the preparation method, which together with the fact that the size of the iron particles is significantly reduced compared to the mixed samples it allows the gas molecules to diffuse more easily to react with the iron oxide. Further studies into the reaction kinetics are important for the design and scale-up of the technology allowing for optimal selection of residence time and operating conditions that would lead to minimized operating and capital costs.

The influence of temperature was evaluated for both reduction and

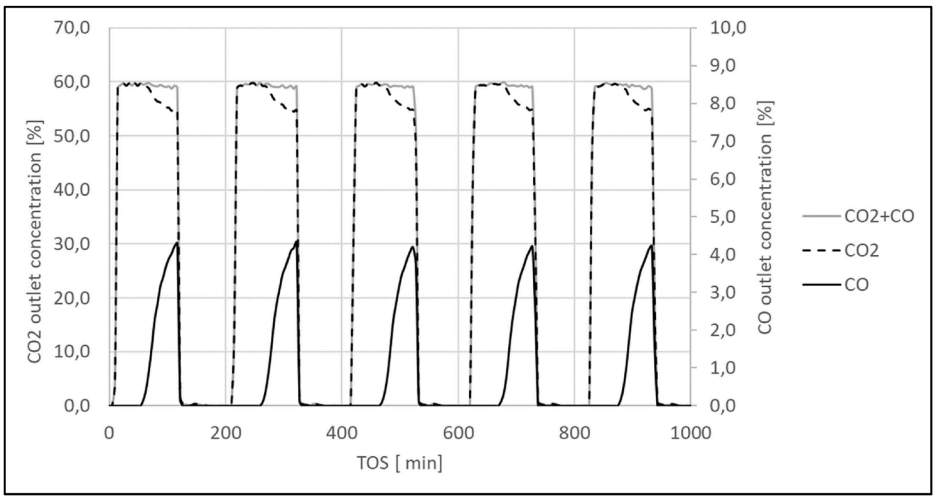

Fig. 22. Transient response of CO and CO_2 concentrations during the first chemical looping step with Sample 4 measured with GC – setting 4.1.

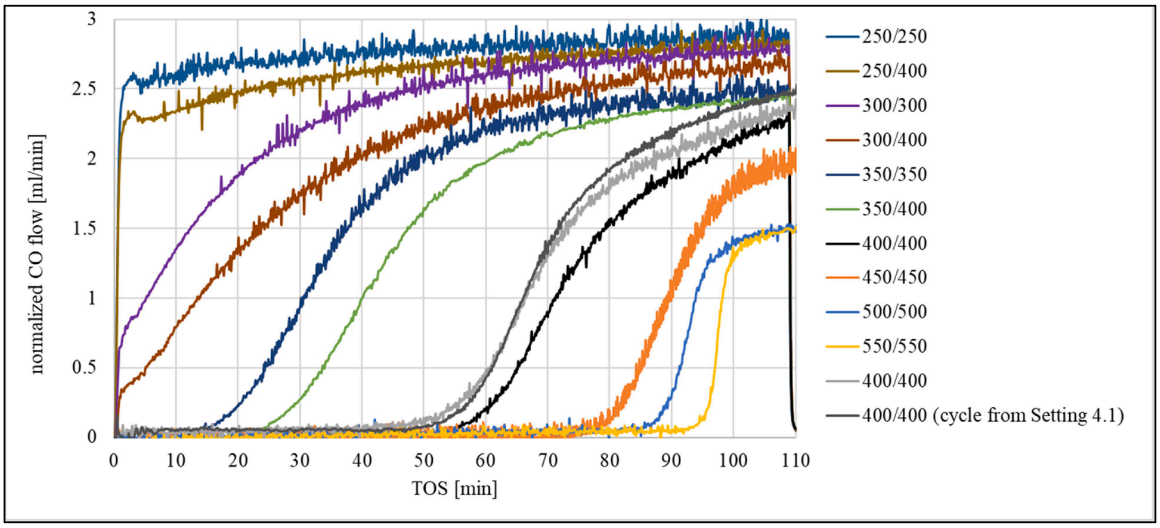

Fig. 23. Influence of temperature on CO conversion on Sample 4- setting 4.2.

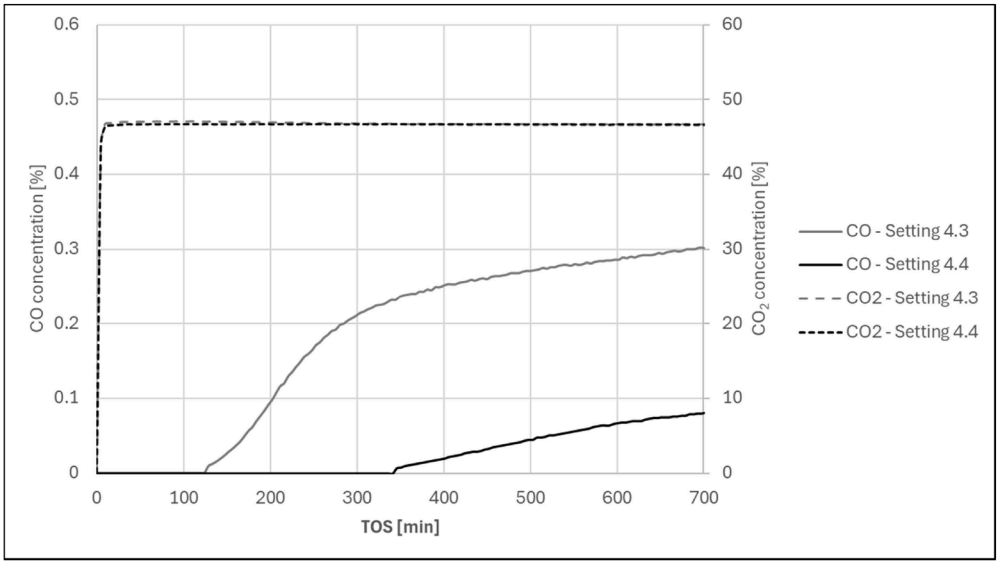

Fig. 24. Transient response of CO and CO_2 concentrations during the first chemical looping step with Sample 4 measured with GC – setting 4.3 and 4.4.

oxidation in the interval from 250 °C to 550 °C. For each temperature, a number of 5 cycles was measured with a reference cycle at 400 °C repeated at the end to check for stability. All measurements for Sample 4 were done using the same material emphasizing the performance and stability over multiple cycles (~200). As seen in Fig. 23 higher temperatures extend the conversion time and show a much sharper transition between high conversion and the moment the CO concentration starts to increase. At temperatures below 350 °C there is no full conversion of CO. Isothermal operation was also evaluated at the lower temperatures ($T < 400$ °C) showing that a higher oxidation temperature is preferred. Going from 350 °C to 400 °C (at the same regeneration temperature) the conversion time is extended by 30 min which is more than double the time in which full conversion is observed at 350 °C. From 400 °C to 450 °C a 30 % extended conversion time can be achieved which means an extra 20 min of complete CO conversion. As the temperature increases, for every 50 °C the extended conversion period is halved which suggests that increasing further the temperature above 550 °C will not significantly improve the performance. Observing the reference 400/400 °C setting it can be seen that the cycle following lower temperatures shows a slight improvement in terms of conversion; when comparing the reference setting at the end of the high temperature settings with one of the initial cycles from Setting 4.1 the performance is the same as seen from the overlay of the grey curves in Fig. 23, highlighting the stability of the process.

Additional measurements were done on Sample 4 with low CO content in the feed to evaluate the performance of the process under more practical conditions. The output of the GC measurements are illustrated in Fig. 24 for a feed of 2000 ppm (setting 4.4) and 4000 ppm CO (setting 4.3). As indicated also by the thermodynamic analysis, the process is not limited at low concentrations. Complete conversion of CO to CO_2 is observed for the first ~130 min for setting 4.3 and 340 min for setting 4.4.

As seen from the thermodynamic and experimental analysis, chemical looping is a promising technology for CO_2 purification capable of reaching the ppm levels of CO rEq.uired by the most stringent CO_2 quality specifications without introducing new impurities. In terms of expected energy consumption, with or without the chemical looping process the CO_2 process needs to be liquefied anyway, so an increase in energy is expected. An additional energy rEq.uirement for the chemical looping process would be the air compression to overcome pressure drops across the reactor during the oxidation step. On the upside, with the chemical looping technology we recover energy content and increase CO_2 recovery compared to liquefaction. Future work will thus focus on a detailed techno-economic evaluation to better highlight the advantages of chemical looping as a CO_2 purification technology from pre-combustion capture.

4. Conclusion

The purity of captured CO_2 is a crucial aspect of CCUS with varying specifications depending on the end-use. This study evaluates the proof of concept of employing chemical looping as a purification method for CO_2-rich streams from pre-combustion capture, targeting CO removal with the perspective of enhanced CO_2 recovery and the simultaneous removal of other impurities like H_2 and CH_4 at reduced energy penalties.

The feasibility of adopting the chemical looping technology for CO removal from a CO_2 rich stream was evaluated from a thermodynamic perspective looking at different possible OC, such as Ni, Cu, Mn, and Fe, at milder conditions ($T < 700$ °C) and lower reducing gas concentrations (e.g., <5 % CO). The most promising redox couples identified are Cu_2O/Cu and Fe_2O_3/Fe_3O_4, while nickel and manganese oxides showed limited feasibility. For the identified redox pairs, both the reduction and the regeneration are exothermic, showing opportunity for heat recovery, which can be integrated in the up-stream capture section as heat (i.e., steam) or converted into electricity. Due to its low HSE risk, availability, reduced cost and acceptable performance, iron-based oxygen carrier was further evaluated experimentally considering different preparation methods with Al_2O_3 as support material. Sample 4, Fe_2O_3 impregnated on Al_2O_3, showed the best performance with high CO conversion period and excellent stability over >100 cycles in the temperature range 400–550 °C. These results successfully validate the proof-of-concept for the chemical looping purification concept. It was observed that high temperatures are favourable for increasing the conversion period but after reaching 450 °C the extended conversion time halves every 50 °C increase. Optimal operating conditions should be determined based on process design (i.e., including heat integration) and economics.

Future work will focus on testing also with H_2 present in the feed, exploring other materials, and perform a technoeconomic evaluation and benchmarking to further assess the attractiveness of the technology for CO_2 product purification.

CRediT authorship contribution statement

Dora-Andreea Chisăliță: Writing – original draft, Investigation, Conceptualization. **Gerard Douwe Elzinga:** Investigation. **Jurriaan Boon:** Writing – review & editing, Conceptualization.

Declaration of competing interest

The authors declare the following financial interests/personal relationships which may be considered as potential competing interests:

Chisalita Dora-Andreea has patent #Patent applied for number P62003754EP (date of filing: 19 / 12 / 2023): CO2 purification by chemical looping pending to TNO. If there are other authors, they declare that they have no known competing financial interests or personal relationships that could have appeared to influence the work reported in this paper.

Acknowledgements

This project has received funding from the Dutch Ministry for Economic Affairs and Climate Policy.

Supplementary materials

Supplementary material associated with this article can be found, in the online version, at doi:10.1016/j.ijggc.2026.104612.

Data availability

Data will be made available on rEq.uest.

References

Abad, A., García-Labiano, F., de Diego, L.F., Gayán, P., Adánez, J., 2007. Reduction Kinetics of Cu-, Ni-, and Fe-Based Oxygen Carriers Using Syngas (CO + H2) for Chemical-Looping Combustion. Energy & Fuels 21, 1843–1853. https://doi.org/10.1021/ef070025k.

Abuelgasim, S., Wang, W., Abdalazeez, A., 2021. A brief review for chemical looping combustion as a promising CO2 capture technology: fundamentals and progress. Sci. Total Environ. 764, 142892. https://doi.org/10.1016/j.scitotenv.2020.142892.

Adanez, J., Abad, A., Garcia-Labiano, F., Gayan, P., de Diego, L.F., 2012. Progress in Chemical-Looping Combustion and Reforming technologies. Prog. Energy Combust. Sci. 38, 215–282. https://doi.org/10.1016/j.pecs.2011.09.001.

Adánez, J., de Diego F., L., García-Labiano, F., Gayán, P., Abad, A., Palacios M., J., 2004. Selection of Oxygen Carriers for Chemical-Looping Combustion. Energy & Fuels 18, 371–377. https://doi.org/10.1021/ef0301452.

Bilsbak, V., 2009. Conditioning of CO2 Coming from a CO2 Capture Process For Transport and Storage Purposes. Norwegian University of Science and Technology.

Brownsort, P.A., 2019. Briefing On Carbon Dioxide Specifications For transport: 1st Report of the Thematic Working Group on: CO2 transport, Storage and Networks. EU CCUS PROJECTS NETWORK.

Cai, R., Krzystowczyk, E., Braunberger, B., Li, F., Neal, L., 2024. Techno-economic analysis of chemical looping air separation using a perovskite oxide sorbent. Int. J. Greenh. Gas Control 132, 104070. https://doi.org/10.1016/j.ijggc.2024.104070.

Chisalita, D.-A., Cormos, C.-C., 2019. Techno-economic assessment of hydrogen production processes based on various natural gas chemical looping systems with

carbon capture. Energy 181, 331–344. https://doi.org/10.1016/j.energy.2019.05.179.
Czakiert, T., Krzywanski, J., Zylka, A., Nowak, W., 2022. Chemical Looping Combustion: a Brief Overview. Energies. https://doi.org/10.3390/en15041563.
Faizal, A., Deshpande, A., 2025. Experimental demonstration of the application of packed bed chemical looping (unmixed) combustion for generating hot liquid utility streams. Therm. Sci. Eng. Prog. 63, 103746. https://doi.org/10.1016/j.tsep.2025.103746.
Fan, L.-S., Zeng, L., Luo, S., 2015. Chemical-looping technology platform. AIChE J. 61, 2–22. https://doi.org/10.1002/aic.14695.
Fennell, P., 2015. Calcium and chemical looping technology: an introduction. Calcium Chem. Looping Technol. Power Gener. Carbon Dioxide 3–14. https://doi.org/10.1016/B978-0-85709-243-4.00001-X. CO.
Gallucci, F., Hamers, H.P., van Zanten, M., van Sint Annaland, M., 2015. Experimental demonstration of chemical-looping combustion of syngas in packed bed reactors with ilmenite. Chem. Eng. J. 274, 156–168. https://doi.org/10.1016/j.cej.2015.03.081.
IEA, 2024. Carbon Capture, Utilisation and Storage - Overview [WWW Document]. URL. https://www.iea.org/energy-system/carbon-capture-utilisation-and-storage.
IPCC, 2023. Summary for Policymakers. In: Lee, H., Romero, J. (Eds.), Climate Change 2023: Synthesis Report. Contribution of Working Groups I, II and III to the Sixth Assessment Report of the Intergovernmental Panel On Climate Change. Core Writing Team, Geneva, Switzerland. https://doi.org/10.59327/IPCC/AR6-9789291691647.001.
Jansen, D., Gazzani, M., Manzolini, G., Dijk, E.van, Carbo, M., 2015. Pre-combustion CO2 capture. Int. J. Greenh. Gas Control 40, 167–187. https://doi.org/10.1016/j.ijggc.2015.05.028.
Jerndal, E., Mattisson, T., Lyngfelt, A., 2006. Thermal Analysis of Chemical-Looping Combustion. Chem. Eng. Res. Des. 84, 795–806. https://doi.org/10.1205/cherd05020.
Khan, M.N., Shamim, T., 2017. Thermodynamic screening of suitable oxygen carriers for a three reactor chemical looping reforming system. Int. J. Hydrogen Energy 42, 15745–15760. https://doi.org/10.1016/J.IJHYDENE.2017.05.037.
Krzystowczyk, E., Haribal, V., Dou, J., Li, F., 2021. Chemical Looping Air Separation Using a Perovskite-Based Oxygen Sorbent: system Design and Process Analysis. ACS Sustain. Chem. Eng. 9, 12185–12195. https://doi.org/10.1021/acssuschemeng.1c03612.
Liu, X.-L., Yin, X.-J., Zhang, H., 2014. Reaction Characteristics of CO and Sintering Ore Used as an Oxygen Carrier in Chemical Looping Combustion. Energy & Fuels 28, 6066–6076. https://doi.org/10.1021/ef5009677.
Liu, Z., Li, Z., Zhang, Yuan, Zhang, Yidian, Zhao, B., 2022. Thermodynamic analysis of using chemical-looping combustion in Allam-Z cycle instead of common combustion. Energy Convers. Manag. 254, 115229. https://doi.org/10.1016/j.enconman.2022.115229.
Lyngfelt, A., 2015. Oxygen carriers for chemical-looping combustion. Calcium Chem. Looping Technol. Power Gener. Carbon Dioxide 221–254. https://doi.org/10.1016/B978-0-85709-243-4.00011-2. CO.
Lyngfelt, A., Brink, A., Langørgen, Ø., Mattisson, T., Rydén, M., Linderholm, C., 2019. 11,000 h of chemical-looping combustion operation—Where are we and where do we want to go? Int. J. Greenh. Gas Control 88, 38–56. https://doi.org/10.1016/J.IJGGC.2019.05.023.
Mattisson, T., García-Labiano, F., Kronberger, B., Lyngfelt, A., Adánez, J., Hofbauer, H., 2007. Chemical-looping combustion using syngas as fuel. Int. J. Greenh. Gas Control 1, 158–169. https://doi.org/10.1016/S1750-5836(07)00023-0.
Mattisson, T., Keller, M., Linderholm, C., Moldenhauer, P., Rydén, M., Leion, H., Lyngfelt, A., 2018. Chemical-looping technologies using circulating fluidized bed systems: status of development. Fuel Process. Technol. 172, 1–12. https://doi.org/10.1016/J.FUPROC.2017.11.016.
Matzen, M., Pinkerton, J., Wang, X., Demirel, Y., 2017. Use of natural ores as oxygen carriers in chemical looping combustion: a review. Int. J. Greenh. Gas Control 65, 1–14. https://doi.org/10.1016/j.ijggc.2017.08.008.
Monteiro, J., Möllenbruck, F., Kamijo, T., Deitert, J., Willms, E., Rudowski, L., Lemke, J., Dijk, E.van, Boon, J., Eijk, S.van, Neele, F.B.T.-D. of C.C. and S, 2024. Chapter two - CO2 capture technologies. In: Rycroft, L. (Ed.), Woodhead Publishing Series On Carbon Capture and Storage. Woodhead Publishing, pp. 25–60. https://doi.org/10.1016/B978-0-323-95498-3.00006-7.
Najera, M., Solunke, R., Gardner, T., Veser, G., 2011. Carbon capture and utilization via chemical looping dry reforming. Chem. Eng. Res. Des. 89, 1533–1543. https://doi.org/10.1016/j.cherd.2010.12.017.
Nandy, A., Loha, C., Gu, S., Sarkar, P., Karmakar, M.K., Chatterjee, P.K., 2016. Present status and overview of Chemical Looping Combustion technology. Renew. Sustain. Energy Rev. 59, 597–619. https://doi.org/10.1016/J.RSER.2016.01.003.
Northern Lights, 2024. Liquid CO2 Quality Specifications.
Outokumpu Research Oy, 2002. HSC Chemistry v5.11.
Porter, R.T.J., Barnett, J., Cobden, E., De Coninck, H., Mahgerefteh, H., Manzolini, G., Martynov, F., Ruggeri, F., Spallina, V., 2021. Challenges and Opportunities of Achieving European Co2 Transportation and Storage Specifications for Carbon Capture in the Iron and Steel Industry. In: SINTEF Proceedings, pp. 174–181.
Porter, R.T.J., Fairweather, M., Pourkashanian, M., Woolley, R.M., 2015. The range and level of impurities in CO2 streams from different carbon capture sources. Int. J. Greenh. Gas Control 36, 161–174. https://doi.org/10.1016/J.IJGGC.2015.02.016.
Ramezani, R., Felice, L.Di, Gallucci, F., 2023. A review of chemical looping reforming technologies for hydrogen production: recent advances and future challenges. J. Phys. Energy 5, 24010. https://doi.org/10.1088/2515-7655/acc4e8.
Shirley, P., Myles, P., 2019. Quality Guidelines for Energy System Studies: CO2 Impurity Design Parameters. United States. https://doi.org/10.2172/1566771.
Tang, M., Xu, L., Fan, M., 2015. Progress in oxygen carrier development of methane-based chemical-looping reforming: a review. Appl. Energy 151, 143–156. https://doi.org/10.1016/j.apenergy.2015.04.017.
Theo, W.L., Lim, J.S., Hashim, H., Mustaffa, A.A., Ho, W.S., 2016. Review of pre-combustion capture and ionic liquid in carbon capture and storage. Appl. Energy 183, 1633–1663. https://doi.org/10.1016/j.apenergy.2016.09.103.
US Department of Commerce, n.d. NIST Chemistry WebBook [WWW Document]. URL https://webbook.nist.gov/chemistry/form-ser/.
Vitali, M., Corvaro, F., Marchetti, B., Terenzi, A., 2022. Thermodynamic challenges for CO2 pipelines design: a critical review on the effects of impurities, water content, and low temperature. Int. J. Greenh. Gas Control 114, 103605. https://doi.org/10.1016/j.ijggc.2022.103605.
Wang, H., Liu, Y., Laaksonen, A., Krook-Riekkola, A., Yang, Z., Lu, X., Ji, X., 2020. Carbon recycling – An immense resource and key to a smart climate engineering: a survey of technologies, cost and impurity impact. Renew. Sustain. Energy Rev. 131, 110010. https://doi.org/10.1016/J.RSER.2020.110010.
Yu, Z., Yang, Y., Yang, S., Zhang, Q., Zhao, J., Fang, Y., Hao, X., Guan, G., 2019. Iron-based oxygen carriers in chemical looping conversions: a review. Carbon Resour. Convers. 2, 23–34. https://doi.org/10.1016/j.crcon.2018.11.004.
Zhao, K., Jia, C., Li, Z., Du, X., Wang, Y., Li, J., Yao, Z., Yao, J., 2023. Recent Advances and Future Perspectives in Carbon Capture, Transportation, Utilization, and Storage (CCTUS) Technologies: a Comprehensive Review. Fuel 351, 128913. https://doi.org/10.1016/j.fuel.2023.128913.
Zhu, X., Imtiaz, Q., Donat, F., Müller, C.R., Li, F., 2020. Chemical looping beyond combustion – a perspective. Energy Environ. Sci. 13, 772–804. https://doi.org/10.1039/C9EE03793D.